

Exceedance and force of centrality for functional data

Poorbita Kundu, Hang Zhou, and Hans-Georg Müller*

Department of Statistics, University of California, Davis, CA 95616, USA

Abstract

Exceedance refers to instances where a dynamic process surpasses given thresholds, e.g., the occurrence of a heat wave. We propose a novel exceedance framework for functional data, where each observed random trajectory is transformed into an exceedance function, which quantifies exceedance durations as a function of threshold levels. An inherent relationship between exceedance functions and probability distributions makes it possible to draw on distributional data analysis techniques such as Fréchet regression to study the dependence of exceedances on Euclidean predictors, e.g., calendar year when the exceedances are observed. We use local linear estimators to obtain exceedance functions from discretely observed functional data with noise and study the convergence of the proposed estimators. New concepts of interest include the force of centrality that quantifies the propensity of a system to revert to lower levels when a given threshold has been exceeded, conditional exceedance functions when conditioning on Euclidean covariates, and threshold exceedance functions, which characterize the size of exceedance sets in dependence on covariates for any fixed threshold. We establish consistent estimation with rates of convergence for these targets. The practical merits of the proposed methodology are illustrated through simulations and applications for annual temperature curves and medfly activity profiles.

Keywords: Activity profiles, Conditional exceedance, Exceedance functions, Fréchet regression, Functional data analysis, Heat waves.

1 Introduction

In an exceedance event a dynamic process crosses a predetermined critical level or threshold. The concept of exceedances has been widely applied across disciplines such as environmental sciences, engineering, finance, and risk assessment. Early studies include [Drufuca and Giugliano \(1977\)](#), who modeled the total duration of exceedances for SO_2 concentration levels in Milan, and [Graham \(1982\)](#), who applied the notion of exceedance duration to investigate wave heights.

*This research was supported in part by NSF Grant DMS-2310450.

In all areas of science, functional data have become increasingly prevalent. They are usually regarded as realizations of a stochastic process that is commonly assumed to have smooth and square integrable trajectories, or alternatively as realizations of random elements in a Hilbert space (Hsing and Eubank, 2015). For a comprehensive review, we refer readers to the monographs by Ramsay and Silverman (2006), Ferraty and Vieu (2006), Horváth and Kokoszka (2012) and the review article Wang et al. (2016). For any function, an exceedance set consists of the elements of the domain where the function values surpass a predetermined threshold. When considering temperature curves, exceedance sets are of interest to quantify the prevalence of high temperatures or high pollution levels. In engineering, exceedance sets aid to quantify the stress imposed on materials. Rather than the specific structure of exceedance sets, in many real-world scenarios the overall duration of an exceedance, i.e. the size of the exceedance sets, is of primary interest. Chang and McKeague (2022) advanced the study of the size of exceedance sets by introducing occupation time curves to analyze wearable device data from the National Health and Nutrition Examination Survey (NHANES), focusing on the conversion of functional data of bounded variation to exceedance sets for a given threshold. Our work extends these ideas by systematically mapping functional data to exceedance functions on a domain of thresholds and connecting these with distributional data analysis and associated concepts such as the force of centrality that we introduce in this paper.

This encompasses a novel framework for functional data that transforms random trajectories into representations that formally have the same constraints as distributions, where each trajectory is mapped to a function that quantifies the size of the exceedance sets in dependence on the threshold level. Instead of the original time domain, the domain of the transformed functions is an interval of thresholds. The resulting exceedance functions, where the exceedance value at a given threshold is quantified as the fraction of the Lebesgue measure of the corresponding exceedance set of the total Lebesgue measure of the domain, formally correspond to (exceedance) survival functions with associated cumulative distribution functions, and we refer to the derivatives of these distribution functions as exceedance densities, as they have the same characteristics as probability density functions.

Following up on the perspective of viewing exceedance functions as having the same formal constraints as survival functions, we introduce the concept of force of centrality as the ratio of the exceedance density to the exceedance survival function at each threshold level, which formally corresponds to a hazard function in dependence on the threshold level. In contrast to a conventional hazard function, higher values are preferable as they indicate reduced propensity to exceed a given threshold level. We then extend these notions to conditional versions in the presence of Euclidean covariates, such as calendar year when considering temperature exceedances. In the presence of covariates, one may also be interested in threshold exceedance functions, where for a given fixed threshold the size of the exceedance sets is considered as a function of the covariate level, quantifying the propensity for an exceedance as the covariate varies. In addition to introducing these concepts, we develop consistent estimators when one starts with a sample of noisy and discretely measured functional data. We obtain the extension to a regression setting by incorporating Euclidean covariates through Fréchet regression (Petersen and Müller, 2019).

The paper is organized as follows. Section 2 introduces the transformation of functional data to exceedance distribution functions and the associated exceedance densities and force of centrality, with estimates in Section 3, where we also establish rates of convergence. Simulation results and data applications are discussed in Sections 5 and 4 respectively, followed by a brief discussion in Section 6. Proofs are provided in Section S1 and additional data illustrations in Section S2 of the supplementary material.

2 Methodology

2.1 Converting functional data to exceedances

Let $Y : \mathcal{T} \rightarrow \mathcal{D} \subset \mathcal{R}$ be a real-valued stochastic process defined on a compact time domain \mathcal{T} with Lebesgue measure $\|\mathcal{T}\|$. The *exceedance set* Δ_Y at threshold value u is defined as

$$\Delta_Y(u) = \{t \in \mathcal{T} \text{ such that } Y(t) \geq u\}, \quad u \in \mathcal{R}.$$

$\Delta_Y(u)$ captures all points in the time domain \mathcal{T} , where the process $Y(t)$ exceeds or equals a specified threshold u . For smaller u , $\Delta_Y(u)$ is a larger subset of the time domain, since it is easier for $Y(t)$ to exceed a lower threshold. Conversely, as u increases, $\Delta_Y(u)$ will generally shrink. For example, in temperature modeling, $\Delta_Y(u)$ might represent time intervals when temperatures exceed a damaging temperature threshold u .

The exceedance sets $\Delta_Y(u)$ provide a localized view of when and where the process exceeds a threshold. However, in many relevant applications, only aggregated information in the form of the total size of $\Delta_Y(u)$ is of interest rather than the actual sets $\Delta_Y(u)$. We focus here on such scenarios and introduce the *exceedance function* S_Y as

$$S_Y(u) = \frac{\lambda\{\Delta_Y(u)\}}{\lambda\{\mathcal{T}\}}, \quad u \in \mathcal{R}, \quad (1)$$

where λ denotes the Lebesgue measure and S_Y quantifies the relative size or duration of the exceedance event for each threshold u . When normalizing the time domain of the functional data to $[0, 1]$, the denominator in (1) is not needed. The size of the exceedance sets is always constrained between 0 and 1 and $S_Y(u)$ is a decreasing function of u , as higher thresholds are accompanied by smaller exceedance sets, which eventually will be of size 0.

Formally, S_Y thus has the characteristics of a survival function and $F_Y(u) = 1 - S_Y(u)$ the characteristics of a distribution function, which we refer to as the *exceedance distribution function* of Y . We require that the exceedance distribution functions are absolutely continuous with respect to Lebesgue measure, so that one can define a derivative $f_Y(u) = (d/du)F_Y(u)$, which has the characteristics of a density function. Analogously, one can define the exceedance quantile function

$$Q_Y(q) = F_Y^{-1}(q) := \inf\{u : F_Y(u) \geq q, \text{ for all } q \in (0, 1)\}.$$

Let \mathcal{W} be the set of finite second moment probability measures on \mathbb{R} ,

$$\mathcal{W} = \{\mu \in \mathcal{P}(\mathbb{R}) : \int_{\mathbb{R}} |x|^2 d\mu(x) < \infty\}, \quad (2)$$

where $\mathcal{P}(\mathbb{R})$ is the set of all probability measures on \mathbb{R} . Here we do not distinguish the different representations of an absolutely continuous probability measure, such as density function, quantile function and distribution function and we write alternatively $d_W(\nu_1, \nu_2)$, $d_W(f_{\nu_1}, f_{\nu_2})$, $d_W(F_{\nu_1}, F_{\nu_2})$ or $d_W(Q_{\nu_1}, Q_{\nu_2})$, where f_ν , F_ν and Q_ν are density, distribution and quantile function of a measure ν . For two probability measures ν_1 and ν_2 with quantile functions Q_{ν_1} and Q_{ν_2} , the 2-Wasserstein distance has the analytical form

$$d_W^2(\nu_1, \nu_2) = \int_0^1 \{Q_{\nu_1}(t) - Q_{\nu_2}(t)\}^2 dt. \quad (3)$$

Since there is a formal correspondence between exceedance functions and probability measures, we may equip these with the 2-Wasserstein metric to quantify their distances. The 2-Wasserstein metric has proved useful in many practical applications involving samples of one-dimensional distributions (Bolstad et al., 2003; Zhang and Müller, 2011).

In survival analysis, the hazard function plays a central role in characterizing time-to-event data by describing the instantaneous risk of an event occurring at a specific time t , given that the event has not yet occurred by t . Formally, the hazard function is defined as $h(t) = \frac{f(t)}{1-F(t)}$, where $f(t)$ is the probability density function of the event times, and $1 - F(t)$ their survival function. The hazard function is widely used and quantifies the rate of occurrence of an event at t , conditional on survival up to that point. Using the formal analogy of exceedance functions (1) with survival functions motivates the definition of the *force of centrality* on a domain of thresholds, which is a sub-domain of \mathbb{R} such that $F_Y(u) < 1$,

$$h_Y(u) = \frac{f_Y(u)}{S_Y(u)} = \frac{f_Y(u)}{1 - F_Y(u)} = -\frac{d}{du}(\log S(u)).$$

Here, $h_Y(u)$ represents the rate at which, for a process Y , the exceedance sets at level u have

reached a size $0 < S_Y(u) \leq 1$, and this size will decline as u increases.

Larger values of $h_Y(u)$ indicate that the process Y has a smaller tendency to exceed thresholds beyond u and thus a smaller tendency to exceed more extreme thresholds, while the opposite is true for smaller values of $h_Y(u)$. Thus, a larger $h_Y(u)$ means the process Y is less prone to exceed more extreme thresholds, which motivates to refer to $h_Y(u)$ as force of centrality. We note here that in survival analysis the survival of patients is negatively affected for larger values of a hazard function, while here a larger value is preferred, especially at thresholds u where the effects of exceeding the threshold are damaging.

2.2 Conditional exceedance

In the context of regression analysis, the data are paired observations (X, Y) , where X represents the covariate and Y the response variable. The primary goal is to understand the relationship between X and Y . This relationship is typically characterized by the regression function $m(x) = \mathbb{E}[Y | X = x]$. When X and Y involve functional data, most existing studies focus on scalar-on-function regression, where the response is a scalar and the covariates are functional data (Cai and Hall, 2006; Hall and Horowitz, 2007; Yuan and Cai, 2010) or on function-on-function regression (Yao et al., 2005b).

In this paper, we focus on the functional-on-vector setting, where Y_i represents functional responses and X_i one-dimensional or multivariate Euclidean predictors, and specifically on scenarios where exceedances are of primary interest. Our approach is to map the functional data to exceedance functions as previously described and to study their dependence on vector predictors. For example, in climate studies, meteorologists may examine how temperature curves over specific periods of the year vary across calendar years. Additionally, understanding how the sizes of exceedance sets for extreme temperatures evolve over time is of particular interest, as such changes may have significant implications. For instance, analyzing the relationship between calendar years and temperature exceedance functions can provide insights into changes in climate patterns. In agriculture, this analysis can reveal the number of growing days (i.e.,

days exceeding the minimum temperature required for plant growth) on one hand, and the number of days with damaging heat (i.e., days exceeding a temperature level that causes plant damage) on the other.

Analytical analogy of exceedance distributions and probability distributions suggests that for relating exceedance distributions with predictors we can use known tools to relate probability distributions as outcomes to vector predictors. One such tool is Fréchet regression (Petersen and Müller, 2019), which targets the conditional expectation

$$Q_{\oplus}(x) = \operatorname{argmin}_{Q \in \mathcal{W}} \mathbb{E} \left(d_{L^2}^2(Q_Y, Q) \mid X = x \right). \quad (4)$$

Here Q_Y denotes the exceedance quantile function associated with functional response Y and \mathcal{W} is as defined in (2). The implementation of the target (4) follows an approach analogous to targeting $E(Y|X = x)$ in Euclidean regression by linear regression and locally linear regression, where we solve the optimization problems (5) and (6) respectively.

$$Q_{\oplus,G}(\cdot, x) = \operatorname{argmin}_{Q \in \mathcal{W}} \mathbb{E} \left(s_G(X, x) d_W^2(Q_Y, Q) \right), \quad (5)$$

with weights in (5) given by $s_G(X, x) := 1 + (X - \mu)^T \Sigma^{-1}(x - \mu)$, is constructed in analogy to linear regression and is referred to as global Fréchet regression.

Alternatively to global Fréchet regression, by modifying the weight function in (5) to incorporate local weights, one can define a local Fréchet regression (Petersen and Müller, 2019) version,

$$Q_{\oplus,L}(\cdot, x) = \operatorname{argmin}_{Q \in \mathcal{W}} \mathbb{E} \left(s_L(X, x, b) d_W^2(Q_Y, Q) \right), \quad (6)$$

with weights $s_L(z, x, b) = \frac{1}{\sigma_0^2} K_b(z - x) [\mu_2 - \mu_1(z - x)]$, where $K_b(z - x) = b^{-1} K((z - x)/b)$ is a kernel function scaled by bandwidth h , $\mu_j := \mathbb{E}[K_b(X - x)(X - x)^j]$ for $j = 0, 1, 2$, and $\sigma_0^2 = \mu_0\mu_2 - \mu_1^2$. Here we assume that the predictor X is one-dimensional, as local Fréchet regression is subject to the curse of dimensionality. An extension to low-dimensional multivariate predictors is also feasible with some straightforward modifications. Local Fréchet regression adopts and

extends the idea of local linear regression for real valued response to the general case with random object responses.

Since we do not distinguish between different representations of the exceedance distribution, the conditional exceedance distribution $F_{\oplus}(\cdot, x)$, exceedance density $f_{\oplus}(\cdot, x)$, exceedance function $S_{\oplus}(\cdot, x)$, and force of centrality $h_{\oplus}(\cdot, x)$ can be obtained from the conditional quantile exceedance function $Q_{\oplus}(\cdot, x)$ as follows:

$$F_{\oplus}(\cdot, x) = Q_{\oplus}^{-1}(\cdot, x) \quad (7)$$

$$f_{\oplus}(\cdot, x) = dF_{\oplus}(\cdot, x)/dx \quad (8)$$

$$S_{\oplus}(\cdot, x) = 1 - F_{\oplus}(\cdot, x) = 1 - Q_{\oplus}^{-1}(\cdot, x) \quad (9)$$

$$h_{\oplus}(\cdot, x) = \frac{f_{\oplus}(\cdot, x)}{S_{\oplus}(\cdot, x)} = \frac{f_{\oplus}(\cdot, x)}{1 - F_{\oplus}(\cdot, x)}. \quad (10)$$

In the presence of covariates, of major interest is the size of exceedance sets as a function of covariate level x for a fixed threshold u , as exceedances may become more or less likely with varying covariate levels. This motivates the definition of the threshold exceedance function

$$\eta_u(x) = |\mathcal{T}| S_{\oplus}(u, x) = |\mathcal{T}| (1 - Q_{\oplus}^{-1}(u, x)), \quad (11)$$

where $|\mathcal{T}|$ represents the total duration of the time domain and $S_{\oplus}(u, x)$ is the conditional exceedance function. Thus the function $\eta_u(x)$ quantifies the extent to which a pre-specified threshold u is exceeded over a given time domain in dependence on the covariate level x . A typical example would be the selection of a critical temperature as threshold u and considering calendar year as covariate x .

3 Estimation and convergence

So far, exceedance functions, exceedance distribution functions, force of centrality and conditional exceedance have been introduced as population-level concepts. In this section, we focus on estimating these population quantities based on observations from random samples $\{Y_i\}_{i=1}^n$. Although functional data theoretically consist of trajectories observed over a continuum, in practice data are usually collected or observed discretely at N_i time points with additional measurement errors. In this common situation, the actual observations for each Y_i are given by

$$\{(t_{ij}, Z_{ij}) \mid Z_{ij} = Y_i(t_{ij}) + \varepsilon_{ij}, j = 1, \dots, N_i\},$$

where ε_{ij} are random copies of ε , with $\mathbb{E}(\varepsilon) = 0$ and $\text{Var}(\varepsilon) = \nu_0^2 < \infty$. We further assume that the measurement errors $\{\varepsilon_{ij}\}_{i,j}$ are independent of Y_i . For simplicity, we assume $N_i = N$ for all $i = 1, \dots, n$ without loss of generality. The results can be extended to the more general scenario where N_i varies, with minor but tedious modifications.

Information from all subjects can be used to estimate population quantities, such as mean and covariance functions. Corresponding estimates have been extensively studied and can be constructed by using kernel or local polynomial smoothing methods (Yao et al., 2005a; Hall et al., 2006; Zhang and Wang, 2016) or alternatively various spline-based approaches (Rice and Wu, 2001; Yao and Lee, 2006; Cai and Yuan, 2011). Since exceedance functions are derived from individual trajectories, we reconstruct individual trajectories directly from the data available for each trajectory by employing local linear smoothing (Müller, 1987; Fan and Gijbels, 1996). For $t \in \mathcal{T}$, the estimate for the i th trajectory $Y_i(t)$ is

$$\hat{Y}_i(t) = \arg \min_{\beta_{i0} \in \mathbb{R}} \frac{1}{N} \sum_{j=1}^N \frac{1}{h} K \left(\frac{t_{ij} - t}{h} \right) \{Z_{ij} - \beta_{i0} - \beta_{i1}(t_{ij} - t)\}^2, \quad (12)$$

where h denotes the bandwidth used for smoothing and K represents the kernel function. We require the following assumptions:

Assumption 1. *The random functions Y_i are positive almost surely and have a second order*

derivative that is bounded uniformly in $i = 1, \dots, n$.

Assumption 2. *The measurement times t_{ij} form a random sample from a distribution on \mathcal{T} with a density function bounded away from 0 and ∞ for each $1 \leq i \leq n$. The functions Y_i and the t_{ij} are independent for $i = 1, \dots, n$ and $j = 1, \dots, N$.*

Assumption 3. *The kernel function K is a density functional defined on $[-1, 1]$, and is Lipschitz continuous with Lipschitz constant L_K .*

Assumption 4. *There exists $\alpha > 2$ such that $\mathbb{E}|\epsilon_{ij}|^\alpha < \infty$.*

Assumption 5. *The bandwidth h satisfies $Nh^3/\log(nN) \rightarrow \infty$.*

Assumptions 1 to 3 are mild conditions commonly used in kernel smoothing methods, while Assumption 4 is necessary to ensure the uniform convergence of the local linear estimator (Zhang and Wang, 2016). Assumption 5 specifies a rate requirement for the bandwidth h and N , which is critical for consistency. Since the exceedance function estimators rely on the reconstructed \hat{Y}_i , the uniform convergence of $|\hat{Y}_i(t) - Y_i(t)|$ is crucial. In the following we use the abbreviation a.s. for almost surely.

Theorem 1. *Under Assumptions 1 to 5, for $h := (\log(Nn)/N)^{1/5}$ it holds that*

$$\sup_{i=1, \dots, n} \sup_{t \in \mathcal{T}} |\hat{Y}_i(t) - Y_i(t)| = O \left(\left(\frac{\log(Nn)}{N} \right)^{2/5} \right) \quad a.s.$$

Theorem 1 establishes the uniform convergence of the reconstructed functions $Y_i(t)$, where the convergence is uniform over both time $t \in \mathcal{T}$ and the subject index i ; this is necessary for subsequent analyses such as Fréchet regression. Under milder assumptions, the following corollary establishes the L^2 convergence rate for each individual trajectory Y_i using standard arguments.

Corollary 1. *Under Assumptions 1 to 3, if the measurement errors ϵ_{ij} have finite second moments, writing $\|g\|_{L^2}^2 = \int g^2(x) dx$ for a square integrable function g and choosing $h = N^{-1/5}$, it holds that*

$$\|\hat{Y}_i - Y_i\|_{L^2}^2 = O_P(N^{-2/5}).$$

Denote the exceedance function for the i th subject (defined in Section 2.1) by $S_i := S_{Y_i}$ and similarly for the exceedance distribution function $F_i := F_{Y_i}$, exceedance density function $f_i := f_{Y_i}$ and force of centrality $h_i := h_{Y_i}$. The corresponding estimates for the S_i , F_i and corresponding quantile functions Q_i are

$$\widehat{S}_i(u) = S_{\widehat{Y}_i}(u) := \lambda(\{t \in \mathcal{T} \text{ such that } \widehat{Y}_i(t) \geq u\}), \quad (13)$$

$$\widehat{F}_i = 1 - \widehat{S}_i, \quad \widehat{Q}_i = \widehat{F}_i^{-1}. \quad (14)$$

Based on Theorem 1 and the definition of exceedance functions, the following theorem demonstrates the uniform convergence of \widehat{S}_i , \widehat{F}_i and \widehat{Q}_i , as defined in (13) and (14).

Theorem 2. *Under the assumptions of Theorem 1, further assuming that $\sup_{i=1,\dots,n} |Y_i'| < \Delta$ for a constant $\Delta > 0$,*

$$\begin{aligned} \sup_{i=1,\dots,n} \sup_{0 \leq u \leq \max |Y_i|} |\widehat{S}_i(u) - S_i(u)| &= O\left(\left(\frac{\log(Nn)}{N}\right)^{2/5}\right) \quad a.s.; \\ \sup_{i=1,\dots,n} \sup_{0 \leq u \leq \max |Y_i|} |\widehat{F}_i(u) - F_i(u)| &= O\left(\left(\frac{\log(Nn)}{N}\right)^{2/5}\right) \quad a.s.; \\ \sup_{i=1,\dots,n} \sup_{q \in [0,1]} |\widehat{Q}_i(q) - Q_i(q)| &= O\left(\left(\frac{\log(Nn)}{N}\right)^{2/5}\right) \quad a.s.. \end{aligned}$$

To estimate the exceedance density f_i , i.e. the derivative of F_i , we consider a positive sequence $\delta_n \rightarrow 0$ as $n \rightarrow \infty$, which we use to construct the estimate $\widehat{f}(u)$ as a difference quotient; we note here that we are not actually dealing with empirical distributions but rather with functions that behave analogously. Then

$$\widehat{f}_i(u) = \frac{\widehat{F}_i(u + \delta_n) - \widehat{F}_i(u - \delta_n)}{2\delta_n}, \quad (15)$$

which gives the estimates for interior points u such that $u \in [\delta_n, 1 - \delta_n]$, while for points in the boundary $u \in [0, \delta_n) \cup (1 - \delta_n, 1]$, $\widehat{f}(u)$ is obtained using forward and backward difference approximations, $\widehat{f}_i(u) = \frac{\widehat{F}_i(u + \delta_n) - \widehat{F}_i(0)}{u + \delta_n}$ and $\widehat{f}_i(u) = \frac{\widehat{F}_i(1) - \widehat{F}_i(u - \delta_n)}{1 - u + \delta_n}$, respectively. This then leads

to the estimates for the force of centrality

$$\hat{h}_i(u) = \frac{\hat{f}_i(u)}{1 - \hat{F}_i(u)}. \quad (16)$$

The following theorem establishes the convergence rate of \hat{f} in dependence on δ_n .

Theorem 3. *In addition to the assumptions of Theorem 1, we assume that F_i has a bounded second-order derivative, where the bound is uniform in i . For any positive sequence δ_n that tends to 0,*

$$\sup_{i=1, \dots, n} \sup_{u \in [\delta_n, 1 - \delta_n]} \left| \hat{f}_i(u) - f_i(u) \right| = O \left(\frac{1}{\delta_n} \left(\frac{\log(Nn)}{N} \right)^{2/5} + \delta_n \right) \quad a.s.$$

Selecting the optimal rate for δ_n , Corollary 2 below establishes the uniform convergence of \hat{f}_i and the estimated force of centrality, uniformly over both the domain (excepting the shrinking boundary regions) and subjects.

Corollary 2. *Under the assumptions of Theorem 3, by choosing $\delta_n = (\log(Nn)/N)^{1/5}$,*

$$\begin{aligned} \sup_{i=1, \dots, n} \sup_{u \in [\delta_n, 1 - \delta_n]} \left| \hat{f}_i(u) - f_i(u) \right| &= O \left(\left(\frac{\log(Nn)}{N} \right)^{1/5} \right) \quad a.s. \\ \sup_{i=1, \dots, n} \sup_{u \in \mathcal{X}_\epsilon} \left| \hat{h}_i(u) - h_i(u) \right| &= O \left(\left(\frac{\log(Nn)}{N} \right)^{1/5} \right) \quad a.s. \end{aligned}$$

We turn now to the important conditional exceedance framework, where one has a Euclidean predictor X and aims to study how exceedances depend on the values of the predictor. Observing that the responses essentially correspond to quantile functions and therefore are subject to the same restrictions as distributional data, we adopt Fréchet regression (Petersen and Müller, 2019), a regression method for scenarios where Euclidean predictors are coupled with responses in general metric spaces, including the Wasserstein space for distributional responses. As mentioned in Section 2.2, one has the choice between a local and a global version of Fréchet regression. In the following we provide convergence results for conditional exceedance

and threshold exceedance functions when using the local version. Similar results can also be obtained for the global version.

For local Fréchet regression one adopts empirical weights derived from local linear regression (Müller, 1987; Fan and Gijbels, 1996) that are given by

$$s_{in}(x, b) = \frac{1}{\hat{\sigma}_0^2} K_b(X_i - x) [\hat{u}_2 - \hat{u}_1(X_i - x)], \quad (17)$$

where $\hat{u}_l = n^{-1} \sum_{i=1}^n K_b(X_i - x)(X_i - x)^l$ for $l \in \{0, 1, 2\}$, $\hat{\sigma}_0^2 = \hat{u}_0 \hat{u}_2 - \hat{u}_1^2$, and $K_b(\cdot) = b^{-1} K(\cdot/b)$. An estimate $\hat{f}_{\oplus, L}(x)$ for the local Fréchet regression conditional exceedance density $f_{\oplus, L}(x)$, which is derived from the conditional exceedance quantile function $Q_{\oplus, L}(x)$ in (6) is then obtained as the density function corresponding to the conditional quantile function estimate

$$\hat{Q}_{\oplus, L}(\cdot, x) = \operatorname{argmin}_{q \in \mathcal{Q}(\Omega_F)} \left\| q - \frac{1}{n} \sum_{i=1}^n s_{in}(x, b) \hat{Q}_i \right\|_{L^2([0,1])}^2. \quad (18)$$

The resulting estimates for the Fréchet regression exceedances can then be equivalently expressed in terms of the exceedance distribution function $\hat{F}_{\oplus, L}(x) = \hat{Q}_{\oplus, L}^{-1}(x)$, the exceedance function $\hat{S}_{\oplus, L}(x) = 1 - \hat{F}_{\oplus, L}(x)$, the exceedance density $\hat{f}_{\oplus, L}(x)$, the force of centrality $\hat{h}_{\oplus, L}(x) = \hat{f}_{\oplus, L}(x) / \{1 - \hat{F}_{\oplus, L}(x)\}$, or the threshold exceedance function $\hat{\eta}_u(x) = |\mathcal{T}| \{1 - \hat{Q}_{\oplus, L}^{-1}(u, x)\}$.

To derive the convergence rate of these estimators, we impose the following assumption, which has been adopted previously in Petersen and Müller (2019).

Assumption 6. *The marginal density of X and the conditional densities of X given the response $\tilde{Q} = q$, denoted by f_X and g_q respectively, exist for $\tilde{Q} \in \mathcal{W}$ and are twice continuously differentiable. The latter holds for all $q \in \mathcal{W}$ (2), with $\sup_{x, q} |g_q''(x)| < \infty$.*

Theorem 4. *Assume the density function of the distribution of the predictors X satisfies $f_X > 0$ and the bandwidth used for local Fréchet regression satisfies $b \asymp n^{-1/5}$. Under Assumptions 1 to 6*

$$d_W(\hat{f}_{\oplus, L}(x), f_{\oplus, L}(x)) = O_P \left(\left(\frac{\log(Nn)}{N} \right)^{2/5} + n^{-2/5} \right).$$

Under additional assumptions presented in the Supplement, the following proposition establishes the uniform convergence of the local Fréchet estimates $\widehat{Q}_{\oplus,L}(\cdot, x)$ in (18), where the proof of this result essentially follows the same lines as the proof of Theorem 1 in [Chen and Müller \(2022\)](#). Corollary 3 shows the convergence rate for the threshold exceedance function $\eta_u(x)$ constructed with local Fréchet regression and is a consequence of the following Proposition 1.

Proposition 1. *Under Assumptions 1 to 6 and Assumptions S1 to S4 in the Supplement, it holds that*

$$\sup_x d_W(\widehat{f}_{\oplus,L}(x), f_{\oplus,L}(x)) = O\left(\left(\frac{\log(Nn)}{N}\right)^{2/5} + n^{-1/(\beta_1+2\beta_2-3+\epsilon)}\right) \quad a.s.$$

for any positive ϵ , where β_1 and β_2 are defined in Assumption S4 in the Supplement.

Corollary 3. *Under the assumptions of Proposition 1, for each fixed threshold u , it holds that*

$$\sup_x |\widehat{\eta}_u(x) - \eta_u(x)| = O\left(\left(\frac{\log(Nn)}{N}\right)^{2/5} + n^{-1/(\beta_1+2\beta_2-3+\epsilon)}\right) \quad a.s.$$

for any positive ϵ , where β_1 and β_2 are defined in Assumption S4 in the Supplement.

To obtain global regression estimates, we adopt the empirical global weights from [Petersen and Müller \(2019\)](#), defined as

$$s_{in}(x) := 1 + (X_i - \bar{X})^T \widehat{\Sigma}^{-1}(x - \bar{X}), \quad (19)$$

where $\bar{X} := n^{-1} \sum_{i=1}^n X_i$ is the sample mean and $\widehat{\Sigma} := n^{-1} \sum_{i=1}^n (X_i - \bar{X})(X_i - \bar{X})^T$ is the sample covariance matrix. We base estimates for the global Fréchet exceedance regression given a Euclidean predictor on estimated quantile functions \widehat{Q}_i in (14). Incorporating the empirical global weights $s_{in}(x)$ leads to

$$\widehat{Q}_{\oplus,G}(\cdot, x) = \operatorname{argmin}_{Q_0 \in \mathcal{Q}(\Omega_F)} \left\| Q_0 - \frac{1}{n} \sum_{i=1}^n s_{in}(x) \widehat{Q}_i \right\|_{L^2([0,1])}^2. \quad (20)$$

Under the assumptions of Theorem 1, it can be shown that the convergence rate for the resulting estimated exceedance densities satisfies

$$d_W(\hat{f}_{\oplus,G}(x), f_{\oplus,G}(x)) = O_P \left(\left(\frac{\log(Nn)}{N} \right)^{2/5} + n^{-1/2} \right),$$

where $d_W(\cdot, \cdot)$ denotes the Wasserstein distance (3).

4 Simulation Study

We demonstrate the applicability of the proposed methodology in recovering latent individual-level exceedance functions through simulation studies in two distinct settings. The general simulation framework follows a standard functional data generation process based on the Karhunen-Loève decomposition. We generate functional data on a regular time grid $\{t_{ij}\}_{j=1}^N \subset \mathcal{T}$, for $i = 1, 2, \dots, n$, with underlying trajectories modeled as $Y_{ij} = \log(1 + e^{V_i(t_{ij})})$, where $V_i(t_{ij}) = \mu(t_{ij}) + \sum_{k=1}^K \xi_{ik} \phi_k(t_{ij})$. The choices of the mean function $\mu(t)$, orthonormal eigenfunctions $\phi_k(t)$, and eigenvalues λ_k are specific to the simulation setting and are described in more detail below. The functional principal components are generated as $\xi_{ik} \sim \mathcal{N}(0, \lambda_k)$ for $k = 1, \dots, K$ and $i = 1, \dots, n$. To mirror real-life data and demonstrate the effect of noise variance ν_0 , we contaminate the true trajectories Y_{ij} with homoscedastic noise $\epsilon_{ij} \stackrel{\text{i.i.d.}}{\sim} \mathcal{N}(0, \nu_0^2)$, resulting in observed values $z_{ij} = Y_{ij} + \epsilon_{ij}$. We evaluate our proposed approach for $N = 100, 200, 500$ observations per subject and noise levels $\nu_0 = 0.05, 0.5, 1$, fixing the time interval as $\mathcal{T} = [0, 1]$. For each (N, ν_0) , the simulation study was performed for $n = 200$ independent units and was repeated $B = 1000$ times.

Setting I: To model multimodal functional trajectories that exhibit high fluctuations (see Figure 1), we use the mean function $\mu(t) = m_0 + 2 \sin(2\pi t) + \sin(4\pi t) + 0.5 \cos(6\pi t)$ and $K = 8$ eigencomponents, incorporating higher-frequency sine and cosine components. Specifically, the eigenfunctions are $\phi_1(t) = \sqrt{2} \sin(2\pi t)$, $\phi_2(t) = \sqrt{2} \cos(2\pi t)$, $\phi_3(t) = \sqrt{2} \sin(4\pi t)$, $\phi_4(t) = \sqrt{2} \cos(6\pi t)$, $\phi_5(t) = \sqrt{2} \sin(8\pi t)$, $\phi_6(t) = \sqrt{2} \cos(10\pi t)$, $\phi_7(t) =$

$\sqrt{2}\sin(12\pi t)$, and $\phi_8(t) = \sqrt{2}\cos(14\pi t)$, with corresponding eigenvalues $\lambda_k = c_0 k^{-a}$ for $k = 1, \dots, 8$. Here the noise is assumed to be heteroscedastic, $\epsilon_{ij} \sim N(0, \nu_0^2(1.5 + \sin(4\pi t_{ij})))$, where $m_0 = 20$, $c_0 = 4$, and $a = 1$.

Setting II: In this relatively simpler setting, we consider the deterministic mean function $\mu(t) = m_0 + 2\sin(2\pi t)$ and include $K = 3$ eigencomponents. The chosen orthonormal eigenfunctions are $\phi_1(t) = \sqrt{2}\sin(2\pi t)$, $\phi_2(t) = \sqrt{2}\cos(2\pi t)$, with corresponding eigenvalues $\lambda_k = c_0 k^{-a}$ for $k = 1, 2, 3$, where $m_0 = 15$, $c_0 = 3$, and $a = 1$.

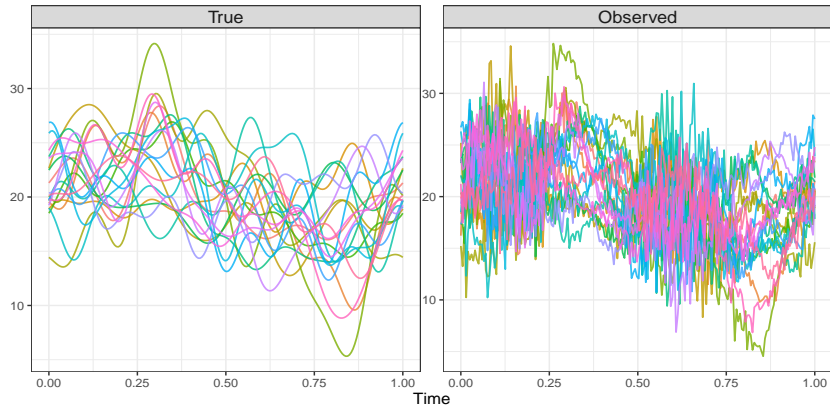


Figure 1: Simulation setting I. True underlying trajectories (left) and observed data (right) for 20 randomly selected subjects and noise variance 1.

In this section, we present the simulation results for Setting I, while the corresponding illustrations for the simpler Setting II are provided in section S2.2 of the supplementary material. To estimate the underlying exceedance functions S_i , we use the estimation methodology described in (13). For the b th replicate with estimate \widehat{S}_i^b , the error is quantified as $d_W^2(S_i, \widehat{S}_i^b)$ based on the corresponding metric defined in Section 2. Averaging over $B = 1000$ simulated datasets, the individual-level root-mean-square errors are given by $\text{RMSE}_i := (B^{-1} \sum_{b=1}^B d_W^2(S_i, \widehat{S}_i^b))^{1/2}$. Table 1 presents the mean error $\overline{\text{RMSE}} := n^{-1} \sum_{i=1}^n \text{RMSE}_i$, illustrating how errors vary with different values of N and noise levels ν_0 . The estimation errors (averaged over $n = 200$ subjects) keep decreasing as the number of observations per subject increases and the errors also reflect changes in noise levels.

Table 1: Individual-level RMSE averaged over 1000 Monte Carlo runs for the estimation of exceedance functions (defined in Section 4) in simulation setting I for $n = 200$ subjects with varying number of observations N available per subject and varying noise level ν_0 . The reported values denote the mean RMSE values averaged over 200 subjects.

N	Noise Level ν_0		
	1.0	0.5	0.05
100	0.851	0.830	0.819
200	0.417	0.370	0.341
500	0.211	0.126	0.072

To assess the finite sample performance of global Fréchet regression estimates, we use the following data generating mechanism. We generate a one-dimensional covariate as $X \sim U(a_0, b_0)$ and $\kappa(x) = a_1 + b_1x + \epsilon_1$, where $\epsilon_1 \sim \mathcal{N}(0, 0.5)$. We use the mean function $\mu(t, x) = \kappa(x)\mu(t)$, where $\mu(t)$ is as defined above. With the same orthonormal basis functions ϕ_k and eigenvalues λ_k as before, we generate the functional principal components $\xi_{ik} \stackrel{\text{ind.}}{\sim} \mathcal{N}(0, \lambda_k)$ for each eigencomponent (indexed by $k = 1, \dots, K$). The individual trajectories are thus generated using Karhunen-Loève expansion, with white noise $\epsilon_{ij} \stackrel{\text{i.i.d.}}{\sim} \mathcal{N}(0, \nu_0^2)$. We choose $m_0 = 2, a_0 = 1, b_0 = 5, a_1 = 1, b_1 = 5$. From the simulated functional data, we obtain the “oracle” conditional exceedance functions (see Section 2 for definition) and their estimated counterparts (methodology stated in Section 3), based on global Fréchet regression on predictor X . A similar generation method is used for local Fréchet regression, where the continuous covariate X is generated from a truncated normal (μ_X, σ_X) with support $[l_X, u_X]$. We further use the non-linear power function $\kappa(x) = a_1 + b_1x + c_1x^{3/2} + \epsilon_1$, wherein we choose $\mu_X = 3, \sigma_X = 0.5, l_X = 1, u_X = 5, a_1 = 10, b_1 = 5, c_1 = 2, m_0 = 4$. Analogous to global Fréchet regression, we obtain the “oracle” local Fréchet regression functions and their estimated counterparts. Figure 2 illustrates results for simulation Setting I simulation for one run over a dense grid of covariate values for $n = 50, N = 50$ and noise level $\nu_0 = 1$. There is close alignment between the oracle and estimated threshold exceedance functions (corresponding conditional exceedance functions depicted in the Supplement Figures S18 and S19).

We also evaluated the out-of-sample prediction error (quantified by the previously defined

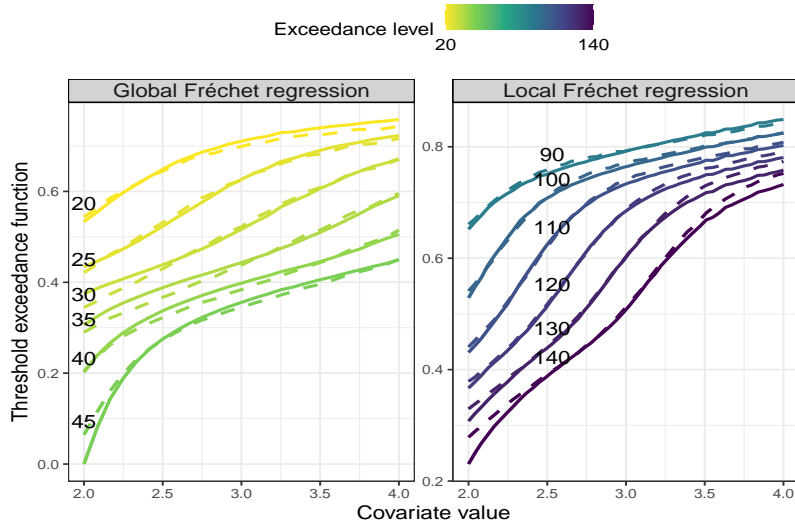


Figure 2: Conditional global (19),(20) (left) and local (17), (18) (right) Fréchet regression functions for one simulation run in simulation setting I. Threshold exceedance functions (response) at varying exceedance levels as a function of covariate value x . The dashed lines represent the “oracle” threshold exceedance functions and the solid lines depict their estimated counterparts.

root-mean-square error) for the conditional exceedance functions obtained from both global and local Fréchet regression. Table 2 summarizes the mean and standard deviation of the RMSE across 500 Monte Carlo simulations for various combinations of sample size n and number of observations per subject N for $B = 500$ simulation runs. As expected, there is a consistent decline of RMSE with increasing N , and for any given N value, the error variability decreases as the sample size grows, however more modestly.

5 Data Applications

5.1 Summer Temperature Data

To illustrate the real-life data application of the proposed exceedance approach, we present an analysis of temperature data recorded in Fort Collins (Colorado) for the months of June through August from 1900 to 1999. The data are available in the extRemes 2.0 package (Gilleland and Katz, 2016) and comprise daily summer temperatures measured in degrees Fahrenheit (see

Table 2: RMSE for conditional exceedance functions obtained from global and local Fréchet regression models (see Sections 2.2 and 4) for simulation setting I with varying number of subjects n and different number of observations N available per subject, at noise level $\nu_0 = 1$. The values indicate the mean RMSE values, averaged over 500 simulation runs, with respective standard errors in the parentheses.

Model	n	N		
		100	200	500
Global	50	1.981 (0.253)	0.987 (0.234)	0.779 (0.230)
	100	1.969 (0.246)	0.961 (0.230)	0.729 (0.213)
	200	1.957 (0.240)	0.932 (0.209)	0.711 (0.212)
Local	50	5.579 (0.329)	2.036 (0.358)	1.307 (0.354)
	100	5.507 (0.221)	1.810 (0.250)	0.940 (0.246)
	200	5.468 (0.156)	1.708 (0.169)	0.705 (0.167)

Figure 3). Temperature data, particularly extremes, are crucial for understanding climate patterns and their potential impacts on human health and ecosystems (Burke et al., 2015; Ebi et al., 2021). We aim to quantify the effects of global warming on maximum and average summer daily temperatures by converting annual temperature profiles to exceedances.

We fit a Fréchet regression model with year as predictor and estimated summer temperature exceedance densities (and analogously force of centrality of centrality) as functional response. Figure 4 demonstrates a rightward shift in the support (and peaks) of the conditional exceedance densities, suggesting a trend of increasing summer temperatures (Davariashtiyani et al., 2023). The conditional force of centrality reflects a similar pattern: For earlier years, the force of centrality tends to rise steeply to assume higher values over a narrower range of temperatures, indicating comparatively cooler summers in the past. The conditional exceedance functions in the bottom panels further illustrate the varying size of the exceedance sets. For each fixed temperature, this function indicates the size of the corresponding exceedance sets, normalized to a fraction between 0 and 1. With increasing calendar years, the size of the exceedance sets is found to increase for all temperatures.

Threshold exceedance functions provide an effective tool to demonstrate the warming effect of climate change by tracking the annual number of summer days that surpass a specified temperature threshold. As illustrated in Figure 5, for an average daily temperature of 70°F,

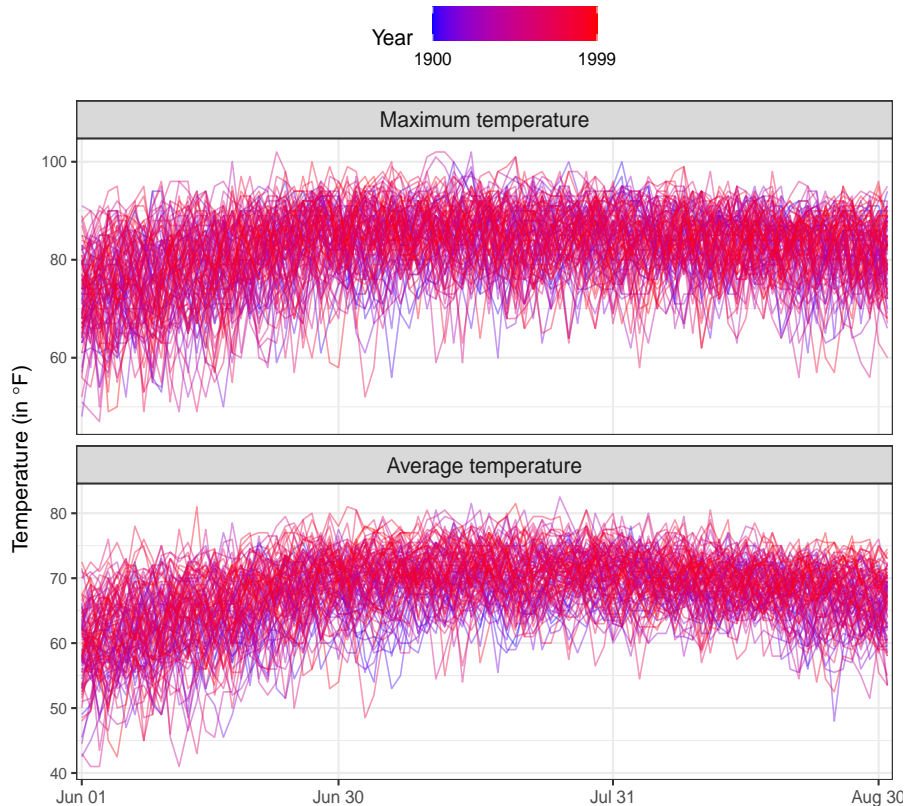


Figure 3: Daily summer temperature data (measured in degree Fahrenheit) recorded at Fort Collins (Colorado) in the months of June-August, for the years 1900 to 1999, where years are colored blue to red. Maximum temperature (top panel) and average temperature (bottom panel).

the threshold exceedance function increases from less than 10 days in 1900 to 50 days in 1999, a very substantial increase. Similarly, fixing the maximum daily temperature at 85°F , the threshold exceedance function shows an increase from less than 20 days to more than 35 days.

5.2 Medfly Activity Profile Data

The analysis of activity profiles and their association with diet and longevity has emerged as a significant area of research in biological and life sciences (Tabacu et al., 2020; Schrack et al., 2023; Chen et al., 2024; Iao et al., 2024). We illustrate our proposed method for medfly activity profile data, with lifetime activity profiles available for 96 female Mediterranean fruit flies (medflies). Each of them was fed with one of the three agar-based gel diets, differing in

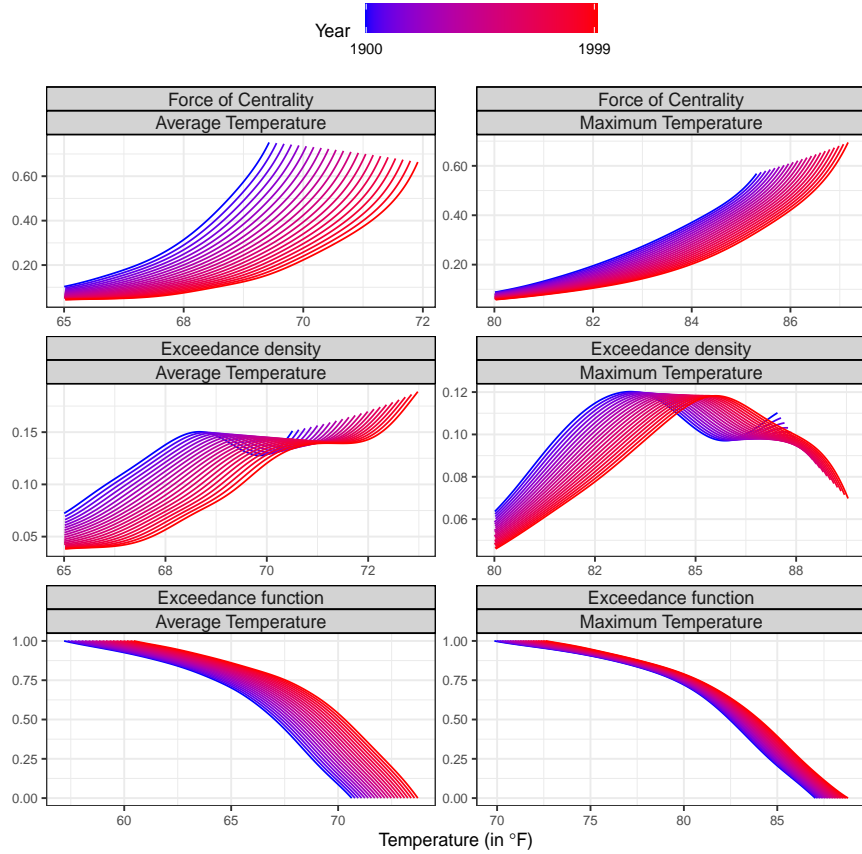


Figure 4: Daily summer temperature data for Fort Collins (Colorado) for 1900 – 1999, with temperature measured in degree Fahrenheit viewed as exceedance levels. Conditional force of centrality (top panel), exceedance densities (middle panel) and exceedance functions (bottom panel) in dependence on calendar year for average temperature (left) and maximum temperature (right), obtained with global Fréchet regression (see (19) and (20)).

their sugar and yeast hydrolysate content (50%, 20% and 10%, represented by treatment C50, C20 and C10 accordingly); every diet group comprised 32 medflies. Each fly was placed in its own glass tube with three infrared light monitors at three different locations. Daily locomotory activity count, defined as the total number of times a fly passed through the middle infrared beam, was recorded every day for each medfly until the death of all medflies (so there is no data censoring), using the Monitor-LAM25 systems. Further details on the experimental setup can be found in [Chen et al. \(2024\)](#).

We focus on medflies that survive through a common age window of $[0, 30]$ days and study their daily locomotory activity in the first 30 days of life, presented in Figure 6. To study

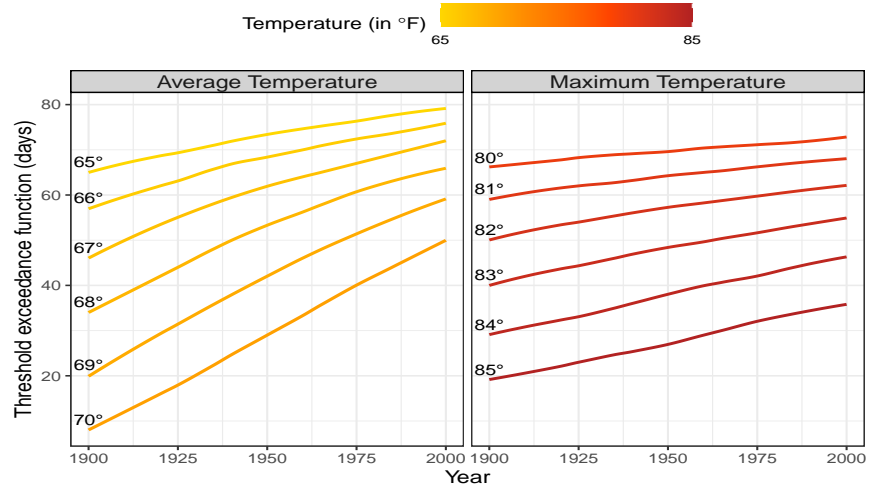


Figure 5: Conditional threshold exceedance functions at different exceedance levels (temperature measured in degree Fahrenheit) as a function of year for average temperature (left) and maximum temperature (right), based on fitted global Fréchet regression model for the daily summer temperature data for Fort Collins.

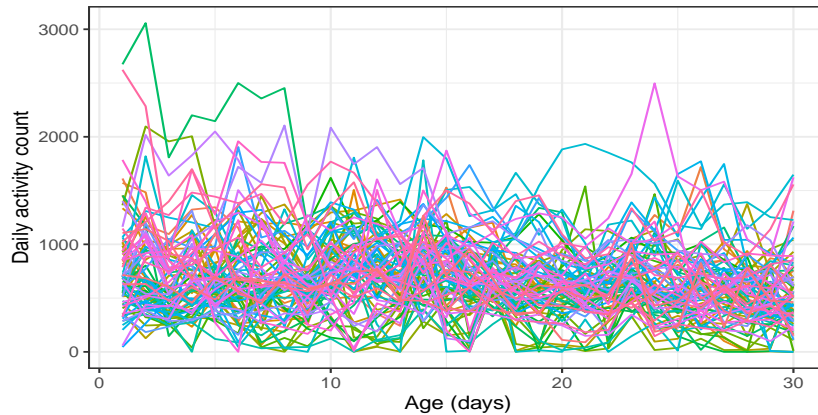


Figure 6: Individual daily activity counts in the first 30 days after eclosion for 80 Mediterranean fruit flies surviving through age 30 in the medfly activity profile study.

the association between activity count and lifespan, quantified as age-at-death, we fit a global Fréchet regression model with estimated force of centrality as functional response and age-at-death as predictor. To account for dietary effects, we further include diet group as an additional predictor.

The conditional force of centrality at varying quantiles of age-at-death is depicted in Figure 7 for each diet group. Within each diet group, longer lived medflies with higher age-at-death

exhibit a force of centrality that rises steeply to higher values over a narrower range of daily activity counts. This illustrates that flies who survive longer are less likely to exceed a given activity count, thereby indicating reduced overall activity in the first 30 days of life for longer-lived flies. The finding aligns with the broader biological concept of trade-offs between energy expenditure and longevity in insects (Chen et al., 2024; Iao et al., 2024). Although the overall patterns remain consistent, there is a distinct effect of diet on daily activity. Specifically, as the sugar-yeast hydrolysate content in the diet increases, the force of centrality tends to take lower values and extends to higher activity levels. This suggests that medflies in the diet group C50 are the most active, followed by C20, and then C10.

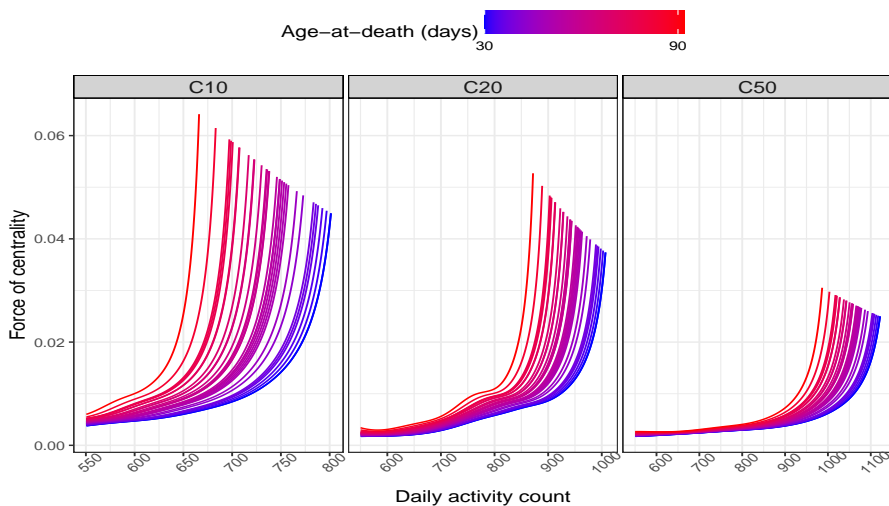


Figure 7: Medfly activity profile study with daily locomotory activity counts viewed as exceedance levels. Conditional force of centrality as a function of age-at-death for the three diet groups with varying glucose-protein concentration: C10 (10%), C20 (20%), and C50 (50%), based on fitted global Fréchet regression model.

A similar pattern is found for the threshold exceedance functions shown in Figure 8. In diet group C10, the number of days (within the first 30 days of life) wherein the activity count exceeds 650 declines from 10 days for flies with a lifespan of 40 to less than 5 days for those surviving until 90. In C20-fed medflies, for an activity count threshold of 850, this decrease is more than 5 days. Among flies fed with C50, at an activity count threshold of 1000, the number of exceedance days decreases from 5 days at an age-at-death of 40 to nearly zero at an

age-at-death of 90.

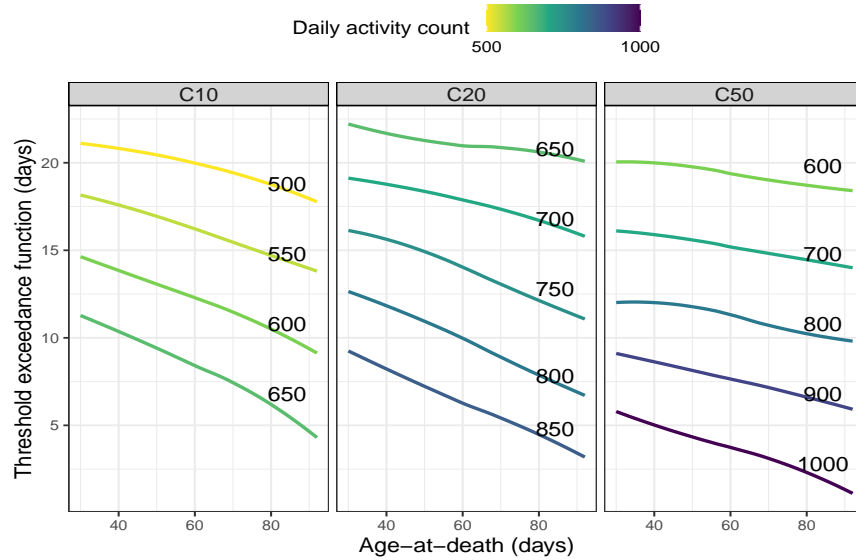


Figure 8: Medfly activity profile study with daily locomotory activity counts viewed as exceedance levels. Conditional threshold exceedance functions at varying activity counts as a function of age-at-death for the three diet groups with varying glucose-protein concentration: C10 (10%), C20 (20%), and C50 (50%), based on fitted global Fréchet regression model.

5.3 NHANES accelerometer data

We further demonstrate the proposed approach for analyzing minute-level accelerometer data from the National Health and Nutrition Examination Survey (NHANES), for approximately 12,000 participants. Viewing physical activity counts as exceedance levels, we examine their relationship with various demographic and socioeconomic covariates, such as age, sex, Body Mass Index (BMI), and Poverty Income Ratio (PIR), with details in Section S2.1 of the supplementary material.

6 Discussion

The proposed exceedance approach that transforms random trajectories into exceedance functions with their formal analogy with survival functions provides a new tool to study extreme

events that occur for dynamic processes within the broader context of functional data. This nonparametric methodology circumvents the challenges of model misspecification associated with traditional distributional exceedance modeling and is underpinned by theory, including uniform convergence rates for individual-level estimates. We introduce the force of centrality that in formal analogy to a hazard function or force of mortality in survival analysis provides comparisons of functional trajectories based on their exceedance behavior. By integrating these concepts with Fréchet regression, the proposed methodology facilitates the analysis of covariate effects on exceedance patterns.

Promising future research directions include an extension to multivariate (vector) functional data, which could illuminate interactions among interdependent exceedance events. Another avenue lies in extending the approach to functional data that have a multivariate time domain. A related topic is to adapt the methodology for spatial and spatiotemporal analysis, where exceedances of random fields are of interest. Another future extension of interest is to incorporate uncertainty quantification.

Supplementary Material for “Exceedance and force of centrality for functional data”

S1 Technical proofs

Proof of Theorem 1. For $r = 0, 1, 2$, denote

$$P_{ir}(t) = \frac{1}{N} \sum_{j=1}^N \frac{1}{h} K\left(\frac{t_{ij} - t}{h}\right) (t_{ij} - t)^r$$

$$Q_{ir}(t) = \frac{1}{N} \sum_{j=1}^N \frac{1}{h} K\left(\frac{t_{ij} - t}{h}\right) (t_{ij} - t)^r Z_{ij}.$$

Then, the solution of optimization (12) has the analytical form:

$$\hat{\beta}_{i0} = \frac{Q_{i0}(t)P_{i2}(t) - Q_{i1}(t)P_{i1}(t)}{P_{i0}(t)P_{i2}(t) - P_{i1}^2(t)}. \quad (21)$$

Thus,

$$\begin{aligned} \hat{Y}_i(t) - Y_i(t) &= \frac{\{Q_{i0}(t) - Y_i(t)P_{i0}(t) - Y_i^{(1)}(t)P_{i1}(t)\}P_{i2}(t)}{P_{i0}(t)P_{i2}(t) - P_{i1}^2(t)} \\ &\quad - \frac{\{Q_{i1}(t) - Y_{i1}(t)P_{i1}(t) - Y_i^{(1)}(t)P_{i2}(t)\}P_{i1}(t)}{P_{i0}(t)P_{i2}(t) - P_{i1}^2(t)}. \end{aligned} \quad (22)$$

We focus on the first term on the right hand side of equation (22). It is not hard to check $P_{i2}(t) = O(1)$ and $P_{i0}(t)P_{i2}(t) - P_{i1}^2(t)$ is bounded away from zero almost surely uniformly in $t \in [0, 1]$ and $i \in 1, \dots, n$ (Zhang and Wang, 2016). Under Assumptions 1 and 3,

$$\begin{aligned} &Q_{i0}(t) - Y_i(t)P_{i0}(t) - Y_i^{(1)}(t)P_{i1}(t) \\ &= \frac{1}{N} \sum_{j=1}^N \frac{1}{h} \mathbf{K} \left(\frac{t_{ij} - t}{h} \right) \{Y_i(t_{ij}) - Y_i(t) - Y_i^{(1)}(t)(t_{ij} - t) + \epsilon_{ij}\} \\ &= \frac{1}{N} \sum_{j=1}^N \frac{1}{h} \mathbf{K} \left(\frac{t_{ij} - t}{h} \right) \epsilon_{ij} + O(h^2). \end{aligned} \quad (23)$$

For the first term in the right hand side of equation (23), let $\chi_N(\gamma)$ be an equidistant grid on $[0, 1]$ with equal grid length $N^{-\gamma}$, where $\gamma > 0$. Let $a_n = \sqrt{\log(Nn)/(Nh)}$.

$$\begin{aligned} \sup_{i=1, \dots, n} \sup_{t \in [0, 1]} \left| \frac{1}{N} \sum_{j=1}^N \frac{1}{h} \mathbf{K} \left(\frac{t_{ij} - t}{h} \right) \epsilon_{ij} \right| &\leq \sup_{i=1, \dots, n} \sup_{t \in \chi(\gamma)} \left| \frac{1}{N} \sum_{j=1}^N \frac{1}{h} \mathbf{K} \left(\frac{t_{ij} - t}{h} \right) \epsilon_{ij} \mathbf{1}_{\{|\epsilon_{ij}| a_n \leq 1\}} \right| \\ &\quad + D_1 + D_2, \end{aligned} \quad (24)$$

with

$$\begin{aligned} D_1 &= \sup_{i=1, \dots, n} \sup_{|t-s| \leq N^{-\gamma}} \left| \frac{1}{N} \sum_{j=1}^N \frac{1}{h} \left\{ \mathbf{K} \left(\frac{t_{ij} - t}{h} \right) - \mathbf{K} \left(\frac{t_{ij} - s}{h} \right) \right\} \epsilon_{ij} \right| \\ &\leq \sup_{i=1, \dots, n} \sup_{|t-s| \leq N^{-\gamma}} \frac{1}{N} \sum_{j=1}^N \frac{1}{h} L_K \frac{|t-s|}{h} |\epsilon_{ij}| \\ &= O \left(\frac{N^{-\gamma}}{h^2} \right) \end{aligned} \quad (25)$$

and

$$\begin{aligned}
D_2 &= \sup_{i=1,\dots,n} \sup_{t \in \chi(\gamma)} \left| \frac{1}{N} \sum_{j=1}^N \frac{1}{h} K \left(\frac{t_{ij} - t}{h} \right) \epsilon_{ij} \mathbb{1}_{\{|\epsilon_{ij}|a_n > 1\}} \right| \\
&\leq \sup_{i=1,\dots,n} \sup_{t \in \chi(\gamma)} \frac{1}{N} \sum_{j=1}^N \frac{1}{h} K \left(\frac{t_{ij} - t}{h} \right) |\epsilon_{ij}| \mathbb{1}_{\{|\epsilon_{ij}|a_n > 1\}} \\
&\leq \sup_{i=1,\dots,n} \frac{\|K\|_\infty}{h} a_n^{\alpha-1} \frac{1}{N} \sum_{j=1}^N |\epsilon_{ij}|^\alpha \\
&= O \left(\frac{a_n^{\alpha-1}}{h} \right).
\end{aligned} \tag{26}$$

The last equalities in equations (25)-(26) are from SLLN and Assumptions 4 and 3. For the first term in the right hand side of equation (24), by Bernstein inequality, for any positive M

$$\begin{aligned}
&\mathbb{P} \left(\sup_{i=1,\dots,n} \sup_{t \in \chi(\gamma)} \left| \frac{1}{N} \sum_{j=1}^N \frac{1}{h} K \left(\frac{t_{ij} - t}{h} \right) \epsilon_{ij} \mathbb{1}_{\{|\epsilon_{ij}|a_n \leq 1\}} \right| \geq Ma_n \right) \\
&\leq nN^\gamma \mathbb{P} \left(\left| \frac{1}{N} \sum_{j=1}^N \frac{1}{h} K \left(\frac{t_{ij} - t}{h} \right) \epsilon_{ij} \mathbb{1}_{\{|\epsilon_{ij}|a_n \leq 1\}} \right| \geq Ma_n \right) \\
&\leq 2nN^\gamma \exp \left(- \frac{M^2 a_n^2 / 2}{\sum_{j=1}^N \mathbb{E} \left[\left\{ \frac{1}{Nh} K \left(\frac{t_{ij} - t}{h} \right) \epsilon_{ij} \mathbb{1}_{\{|\epsilon_{ij}|a_n \leq 1\}} \right\}^2 \right] + Ma_n \|K\|_\infty a_n^{-1} / (3Nh)} \right) \\
&\leq 2nN^\gamma \exp \left(- \frac{M^2 a_n^2 / 2}{\|K\|_\infty^2 \mathbb{E}(\epsilon^2) / Nh + M \|K\|_\infty / (3Nh)} \right) \\
&\leq 2nN^\gamma \exp \left(- \frac{M^2 \log(Nn) / 2}{\|K\|_\infty^2 \mathbb{E}(\epsilon^2) + M \|K\|_\infty / 3} \right) \\
&\leq 2n^{-2} N^{-2},
\end{aligned} \tag{27}$$

where by Assumptions 2 and 3, $\mathbb{E} \left[\left(K \left(\frac{t_{ij} - t}{h} \right) \epsilon_{ij} \right)^2 \right] \leq h \|K\|_\infty^2 \mathbb{E}(\epsilon^2)$. The last inequality holds for large enough M , such that $3M^2 / (6\|K\|_\infty^2 \mathbb{E}(\epsilon^2) + 2M\|K\|_\infty) \geq \max\{3, \gamma + 2\}$.

Thus, by Borel–Cantelli lemma,

$$\sup_{i=1,\dots,n} \sup_{t \in \chi(\gamma)} \left| \frac{1}{N} \sum_{j=1}^N \frac{1}{h} K \left(\frac{t_{ij} - t}{h} \right) \epsilon_{ij} \mathbb{1}_{\{|\epsilon_{ij}|a_n \leq 1\}} \right| = O(a_n) \text{ a.s..} \tag{28}$$

Let $h = (\log(Nn)/N)^{1/5}$. Combining equations (24), (25), (26), and (28) by a similar analysis

as in Section D.1 of [Zhang and Wang \(2016\)](#), under Assumption 5 and for sufficiently large γ , one has $D_r = o(a_n)$ for $r = 1, 2$. Thus

$$\sup_{i=1, \dots, n} \sup_{t \in [0, 1]} \left| Q_0(t) - Y_i(t)P_0(t) - Y_i^{(1)}(t) \right| = O(a_n + h^2) \text{ a.s..}$$

Similar arguments can show that the second term in the right hand side of (22) has the same convergence rate, which completes the proof.

Proof of Theorem 2. To simplify the notation, denote $b_n = (\log(Nn)/N)^{2/5}$. Given

$$\sup_i \sup_t |\hat{Y}_i(t) - Y_i(t)| = O(b_n), \quad \text{a.s.,}$$

this implies that

- If $\hat{Y}_i(t) > u + b_n$, then $Y_i(t) > u$.
- If $Y_i(t) > u + b_n$, then $\hat{Y}_i(t) > u$.

Thus, the set $\{t : \hat{Y}_i(t) > u + b_n\}$ is contained within $\{t : Y_i(t) > u\}$, and similarly, the set $\{t : Y_i(t) > u + b_n\} \subset \{t : \hat{Y}_i(t) > u\}$. Therefore, we have the following inclusions:

$$\{t : \hat{Y}_i(t) > u + b_n\} \subseteq \{t : Y_i(t) > u\} \subseteq \{t : \hat{Y}_i(t) > u - b_n\}$$

$$\{t : Y_i(t) > u + b_n\} \subseteq \{t : \hat{Y}_i(t) > u\} \subseteq \{t : Y_i(t) > u - b_n\}$$

In what follows, we abbreviate $\lambda(\{t : Y_i(t) > u\})$ as $\lambda(Y_i > u)$ for brevity. Taking the Lebesgue measure of these sets gives:

$$\lambda(\{Y_i > u + 2b_n\}) \leq \lambda(\{\hat{Y}_i > u + b_n\}) \leq \lambda(\{Y_i > u\}) \leq \lambda(\{\hat{Y}_i > u - b_n\}) \leq \lambda(\{Y_i > u - 2b_n\})$$

$$\lambda(\{Y_i > u + b_n\}) \leq \lambda(\{\hat{Y}_i > u\}) \leq \lambda(\{Y_i > u - b_n\})$$

For any u ,

$$\begin{aligned} & |\lambda(\hat{Y}_i > u) - \lambda(Y_i > u)| \\ & \leq \max \left\{ \lambda(\hat{Y}_i > u - b_n) - \lambda(\hat{Y}_i > u + b_n), \lambda(Y_i > u - b_n) - \lambda(Y_i > u + b_n) \right\}, \end{aligned}$$

where again, $\lambda(\hat{Y}_i > u - b_n) - \lambda(\hat{Y}_i > u + b_n) \leq \lambda(Y_i > u - 2b_n) - \lambda(Y_i > u + 2b_n)$. Since the function $\lambda(Y_i(t) > u)$ is non-increasing with respect to u , the difference $\lambda(Y_i(t) > u - b_n) - \lambda(Y_i(t) > u + b_n)$ is non-negative and bounded by the measure of the set $\{t : u - b_n < Y_i(t) \leq u + b_n\}$. Hence, the overall bound is:

$$\sup_i \sup_u |\lambda(\hat{Y}_i > u) - \lambda(Y_i > u)| \leq 2 \sup_i \sup_u \lambda(\{t : u - 2b_n < Y_i(t) \leq u + 2b_n\}).$$

For any measurable set A and function f , by the change of variables formula for Lebesgue integrals,

$$\int_{Y_i(A)} f(y) dy = \int_A f(Y_i(t)) Y_i'(t) dt.$$

Let $f(y)$ be the function such that $f(Y_i(t)) = 1/Y_i'(t)$. Then,

$$\lambda(A) = \int_A \mathbb{1} dt = \int_{Y_i(A)} f(y) dy.$$

Since $f(y)$ is bounded by $\|Y_i'\|_\infty^{-1}$, and under the assumption that $|Y_i'| \geq \delta$ almost surely, set $A = \{t : u - 2b_n < Y_i(t) \leq u + 2b_n\}$,

$$\lambda(A) \leq \lambda(Y_i(A)) \delta^{-1} = O(b_n),$$

which completes the proof.

Proof of Theorem 3. By the definition of \hat{f} ,

$$\begin{aligned} \left| \hat{f}_i(u) - f_i(u) \right| &= \frac{\hat{F}_i(u + \delta_n) - \hat{F}_i(u - \delta_n) - \{F_i(u + \delta_n) - F_i(u - \delta_n)\}}{2\delta_n} \\ &\quad + \frac{\{F_i(u + \delta_n) - F_i(u - \delta_n)\}}{2\delta_n} - \frac{dF_i(u)}{du}. \end{aligned} \quad (29)$$

For the first term in the right hand side of equation, by Theorem 2,

$$\begin{aligned} &\sup_{i=1, \dots, n} \sup_{u \in [\delta_n, 1-\delta_n]} \left| \frac{\hat{F}_i(u + \delta_n) - \hat{F}_i(u - \delta_n) - \{F_i(u + \delta_n) - F_i(u - \delta_n)\}}{2\delta_n} \right| \\ &= \sup_{i=1, \dots, n} \sup_{u \in [\delta_n, 1-\delta_n]} \left| \frac{\hat{F}_i(u + \delta_n) - F_i(u + \delta_n) - \{\hat{F}_i(u - \delta_n) - F_i(u - \delta_n)\}}{2\delta_n} \right| \\ &= O\left(\frac{1}{\delta_n} \left(\frac{\log(Nn)}{N}\right)^{2/5}\right), \quad \text{a.s.} \end{aligned} \quad (30)$$

By Taylor expansion,

$$\begin{aligned} F_i(u + \delta_n) &= S(u) + F'_i(u)\delta_n + \frac{\delta_n^2}{2}F''_i(u_1^*) + o(\delta_n^2) \\ F_i(u - \delta_n) &= F_i(u) - F'_i(u)\delta_n + \frac{\delta_n^2}{2}F''_i(u_2^*) + o(\delta_n^2), \end{aligned}$$

where u_1^* and u_2^* are in $[0, 1]$. Then, the second term in the right hand side of (29) becomes

$$\begin{aligned} &\sup_{i=1, \dots, n} \sup_{u \in [\delta_n, 1-\delta_n]} \left| \frac{F_i(u + \delta_n) - F_i(u - \delta_n)}{2\delta_n} - \frac{dF_i(u)}{du} \right| \\ &\leq \sup_{i=1, \dots, n} \sup_{u \in [\delta_n, 1-\delta_n]} \frac{|F''_i(u_1^*) - F''_i(u_2^*)|}{4} \delta_n \\ &\leq \sup_{i=1, \dots, n} \sup_{u \in [\delta_n, 1-\delta_n]} \frac{|F''_i(u_1^*)| + |F''_i(u_2^*)|}{4} \delta_n \\ &= O(\delta_n), \end{aligned} \quad (31)$$

where the last equality is by the assumption F_i has bounded second order derivative in i . The proof is complete by combing equation (29) to (31).

Proof of Corollary 2. The first two statements are easy to verify and for the convergence rate of hazard function \hat{h}_i , note that

$$\hat{h}_i(u) - h_i(u) = \frac{\hat{f}_i(u)}{1 - \hat{F}_i(u)} - \frac{f_i(u)}{1 - F_i(u)} = \frac{\hat{f}_i(u)(1 - F_i(u)) - f_i(u)(1 - \hat{F}_i(u))}{(1 - F_i(u))(1 - \hat{F}_i(u))}. \quad (32)$$

For the denominator in (32), on the set \mathcal{X}_ϵ , one has $(1 - F_i(u))^{-1} \leq 1/\epsilon$ and $|1 - \hat{F}_i(u)|^{-1} \leq \epsilon^{-1}(1 + o(1))$ a.s. by the first statement. Then by Corollary 2

$$\begin{aligned} & \sup_i \left| \frac{\hat{f}_i(u)(1 - F_i(u)) - f_i(u)(1 - \hat{F}_i(u))}{(1 - F_i(u))(1 - \hat{F}_i(u))} \right| \\ &= \sup_i \left| \frac{\hat{f}_i(u) - f_i(u) + \hat{F}_i(u)(f_i(u) - \hat{f}_i(u)) + \hat{f}_i(u)(\hat{F}_i(u) - F_i(u))}{(1 - F_i(u))(1 - \hat{F}_i(u))} \right| \\ &= O\left(\left(\frac{\log(Nn)}{N}\right)^{1/5}\right) \quad \text{a.s.}, \end{aligned}$$

which completes the proof.

Proof of Theorem 4. Let

$$\tilde{Q}_{\oplus, L}(x) = \operatorname{argmin}_{q \in \mathcal{Q}(\Omega_F)} \left\| q - \frac{1}{n} \sum_{i=1}^n s_{in}(x, b) Q_i \right\|_{L^2([0,1])}^2 \quad (33)$$

and $\tilde{f}_{\oplus, L}$ denote the density function of $\tilde{Q}_{\oplus, L}(x)$. By triangle inequality,

$$d_W \left(f_{\oplus, L}(x), \hat{f}_{\oplus, L}(x) \right) \leq d_W \left(f_{\oplus, L}(x), \tilde{f}_{\oplus, L}(x) \right) + d_W \left(\tilde{f}_{\oplus, L}(x), \hat{f}_{\oplus, L}(x) \right). \quad (34)$$

For the last term in the right hand side of last equation, Corollary 1 in Petersen and Müller (2019) shows that under Assumption 6 with $b \asymp n^{-1/5}$,

$$d_W \left(f_{\oplus, L}(x), \widetilde{f_{\oplus, L}}(x) \right) = O_P(n^{-2/5}). \quad (35)$$

For the first term in the right hand side of (34), by the properties of orthogonal projection

on a closed and convex subset in Hilbert space $\mathcal{L}^2([0, 1])$,

$$\begin{aligned}
d_W \left(\tilde{f}_{\oplus, L}(x), \hat{f}_{\oplus, L}(x) \right) &\leq \frac{1}{n} \sum_{i=1}^n |s_{in}(x, b)| \left\| Q_i - \hat{Q}_i \right\|_{L^2([0,1])} \\
&\leq n^{-1} \sum_{i=1}^n |s_{in}(x, b) - s_i(x, b)| \left\| \hat{Q}_i - Q_i \right\|_{L^2([0,1])} + n^{-1} \sum_{i=1}^n |s_i(x, b)| \left\| \hat{Q}_i - Q_i \right\|_{L^2([0,1])} \\
&\leq W_{0n} n^{-1} \sum_{i=1}^n K_b(X_i - x) \left\| \hat{Q}_i - Q_i \right\|_{L^2([0,1])} \\
&\quad + W_{1n} n^{-1} \sum_{i=1}^n K_b(X_i - x) |X_i - x| \left\| \hat{Q}_i - Q_i \right\|_{L^2([0,1])} \\
&\quad + |\mu_2/\sigma_0^2| n^{-1} \sum_{i=1}^n K_b(X_i - x) \left\| \hat{Q}_i - Q_i \right\|_{L^2([0,1])} \\
&\quad + |\mu_1/\sigma_0^2| n^{-1} \sum_{i=1}^n K_b(X_i - x) |X_i - x| \left\| \hat{Q}_i - Q_i \right\|_{L^2([0,1])},
\end{aligned} \tag{36}$$

where $W_{0n} = \hat{\nu}_2/\hat{\sigma}_0^2 - \mu_2/\sigma_0^2$ and $W_{1n} = \hat{\nu}_1/\hat{\sigma}_0^2 - \mu_1/\sigma_0^2$. As shown in [Petersen and Müller \(2019\)](#), $W_{0n} = O_p((nb)^{-1/2})$ and $W_{1n} = O_p((nb^3)^{-1/2})$. Thus, the right-hand side of (36) is dominated by the last two terms. By [Corollary 2](#), one has

$$n^{-1} \sum_{i=1}^n K_h(X_i - x) \left\| \hat{Q}_i - Q_i \right\|_{L^2([0,1])} = O_P \left(\left(\frac{\log(Nn)}{N} \right)^{2/5} \right)$$

and

$$n^{-1} \sum_{i=1}^n K_h(X_i - x) |X_i - x| \left\| \hat{Q}_i - Q_i \right\|_{L^2([0,1])} = O_P \left(\left(\frac{\log(Nn)}{N} \right)^{2/5} \right).$$

Thus,

$$d_W \left(\tilde{f}_{\oplus, L}(x), \hat{f}_{\oplus, L}(x) \right) = O_P \left(\left(\frac{\log(Nn)}{N} \right)^{2/5} \right). \tag{37}$$

The proof is complete by combing (34), (35) and (37).

To obtain the uniform convergence in [Propotion 1](#), we shall introduce the following notations and assumptions. Recall $Q_{\oplus}(\cdot, x)$ is the population and empirical local Fréchet mean

defined by

$$Q_{\oplus,L}(\cdot, x) = \operatorname{argmin}_{q \in \mathcal{W}} L_b(q, x) \quad L_b(q, x) = \mathbb{E} \left(s(X, x, b) d_W^2(Q_Y, q) \right)$$

and

$$\hat{Q}_{\oplus,L}(\cdot, x) = \operatorname{argmin}_{q \in \mathcal{W}} \hat{L}_b(q, x) \quad \hat{L}_b(q, x) = \frac{1}{n} \sum_{i=1}^n s(X_i, x, b) d_W^2(\hat{Q}_{Y_i}, q).$$

Moreover, define the conditional mean $Q_{\oplus}^o(\cdot, x)$ as

$$Q_{\oplus,L}^o(\cdot, x) = \operatorname{argmin}_{q \in \mathcal{W}} L^o(q, x) \quad L^o(q, x) = \mathbb{E} \left[d_W^2(Q_Y, q) \mid X = x \right].$$

The following additional assumptions are needed to establish the consistency of the threshold exceedance function estimates. We require these assumptions in order to be able to apply the uniform convergence results in Theorem 1 of [Chen and Müller \(2022\)](#).

Assumption S7. *For all x in the covariate domain, the minimizers $Q_{\oplus,L}^o(\cdot, x)$, $Q_{\oplus,L}(\cdot, x)$ and $\hat{Q}_{\oplus,L}(\cdot, x)$ exist and are unique, the last P -almost surely. In addition, for any $\epsilon > 0$,*

$$\begin{aligned} \inf_x \inf_{d_W(Q_{\oplus,L}^o(\cdot, x), q) > \epsilon} (L^o(q, x) - L^o(Q_{\oplus,L}^o(\cdot, x), x)) &> 0, \\ \liminf_{b \rightarrow 0} \inf_x \inf_{d_W(Q_{\oplus,L}(\cdot, x), q) > \epsilon} (L_b(q, x) - L_b(Q_{\oplus,L}(\cdot, x), x)) &> 0, \end{aligned}$$

and there exists $c = c(\epsilon) > 0$ such that

$$P \left(\inf_x \inf_{d_W(\hat{Q}_{\oplus,L}(\cdot, x), x) > \epsilon} \left(\hat{L}_b(q, x) - \hat{L}_b \left(Q_{\oplus,L}^o(\cdot, x), t \right) \right) \geq c \right) \rightarrow 1$$

Assumption S8. *Let $B_r(Q_{\oplus,L}^o(\cdot, x)) \subset \mathcal{W}$ be a ball of radius r centered at $Q_{\oplus,L}^o(\cdot, x)$ and*

$$N(\epsilon, B_r(Q_{\oplus,L}^o(\cdot, x)), d_W)$$

be its covering number using balls of radius ϵ . Then

$$\int_0^1 \sup_x \sqrt{1 + \log N(r\epsilon, B_r(Q_{\oplus, L}^o(\cdot, x)), d_{\mathcal{M}})} d\epsilon = O(1), \quad \text{as } r \rightarrow 0+,$$

where $N(\epsilon, B_r, d_W)$ is the minimal number of balls with radius ϵ needed to cover B_r under the d_W metric.

Assumption S9. There exists $r_1, r_2 > 0, c_1, c_2 > 0$ and $\beta_1, \beta_2 > 1$ such that

$$\begin{aligned} \inf_x \inf_{d_W(q, Q_{\oplus, L}^o(\cdot, x)) < r_1} [L^o(q, x) - L^o(Q_{\oplus, L}^o(\cdot, x), x) - c_1 d_W(q, Q_{\oplus, L}^o(\cdot, x))^{\beta_1}] &\geq 0, \\ \liminf_{b \rightarrow 0} \inf_x \inf_{d_W(q, Q_{\oplus, L}(\cdot, x)) < r_2} [L_b(q, x) - L_b(Q_{\oplus, L}(\cdot, x), x) - c_2 d_W(q, Q_{\oplus, L}(\cdot, x))^{\beta_2}] &\geq 0. \end{aligned}$$

Assumption S10. The bandwidth b satisfies $b \asymp n^{-(\beta_1-1)/(2\beta_1+4\beta_2-6+2\epsilon)}$, where ϵ is the positive constant in Proposition 1.

Proof of Proposition 1 By similar arguments as in the proof of Theorem 4,

$$\sup_x d_W(f_{\oplus, L}(x), \widehat{f}_{\oplus, L}(x)) \leq \sup_x d_W(f_{\oplus, L}(x), \widetilde{f}_{\oplus, L}(x)) + \sup_x d_W(\widetilde{f}_{\oplus, L}(x), \widehat{f}_{\oplus, L}(x)), \quad (38)$$

where $\widetilde{f}_{\oplus, L}(x)$ is the minimizer of 33. For the first term on the right-hand side of equation (38), Theorem 1 of Chen and Müller (2022) shows that, under Assumptions 1 to 6 and Assumptions S7 to S10. Corollary 3 shows the convergence rate for the threshold exceedance function $\eta_u(x)$, which follows directly from Proposition 1.,

$$\sup_x d_W(f_{\oplus, L}(x), \widetilde{f}_{\oplus, L}(x)) = O(n^{-1/(\beta_1+2\beta_2-3+\epsilon)}),$$

for all positive ϵ almost surely. The proof is complete by applying similar arguments as in (36) to the second term in the right hand side of (38)

$$\begin{aligned}
& \sup_x d_W \left(\tilde{f}_{\oplus,L}(x), \hat{f}_{\oplus,L}(x) \right) \\
& \lesssim \sup_x |\mu_2/\sigma_0^2| n^{-1} \sum_{i=1}^n K_b(X_i - x) \left\| \hat{Q}_i - Q_i \right\|_{L^2([0,1])} \\
& \quad + \sup_x |\mu_1/\sigma_0^2| n^{-1} \sum_{i=1}^n K_b(X_i - x) |X_i - x| \left\| \hat{Q}_i - Q_i \right\|_{L^2([0,1])} \\
& = O \left(\left(\frac{\log(Nn)}{N} \right)^{2/5} \right),
\end{aligned}$$

where the last equality is from Lemma S.4.2 in [Shao et al. \(2022\)](#) and Theorem 3.

S2 Additional data illustrations

S2.1 NHANES accelerometer data

The National Health and Nutrition Examination Survey (NHANES) is an ongoing study conducted by the U.S. Centers for Disease Control and Prevention (CDC) that aims to assess the health and nutritional status of the non-institutionalized U.S. population. Conducted in biennial cycles, NHANES collects comprehensive data from approximately 10,000 participants per wave. The data are publicly available. Our analysis utilizes data from the 2011 – 2012 and 2013 – 2014 cohorts, during which participants were equipped with wrist-worn physical activity monitors (Actigraph GT3X+) for a duration of seven consecutive days. The raw 80 Hz tri-axial acceleration data collected from these devices were processed into Monitor Independent Movement Summary (MIMS) units. MIMS units serve as a standardized metric for quantifying physical activity levels, derived from raw acceleration measurements to provide a device-independent summary that facilitates cross-study comparisons ([Crainiceanu et al., 2024](#)).

We used the single-level version of the data that includes about 12,000 participants. For each participant with seven consecutive days of minute-level accelerometer data, the data was

compressed by taking the average at each minute across available days, resulting in 1,440 observations per participant, as depicted in Figure S9. The data include various predictors, including age (in years), biological sex, Body Mass Index (BMI), and Poverty Income Ratio (PIR). BMI, defined as the ratio of weight (in kilograms) to height (in meters squared), serves as an indicator of body fitness and potential health risks. PIR, representing the ratio of family income to the poverty threshold, is a measure of socioeconomic status. Further details on the NHANES data can be found at https://www.cdc.gov/nchs/nhanes/?CDC_AAref_Val=https://www.cdc.gov/nchs/nhanes/index.htm.

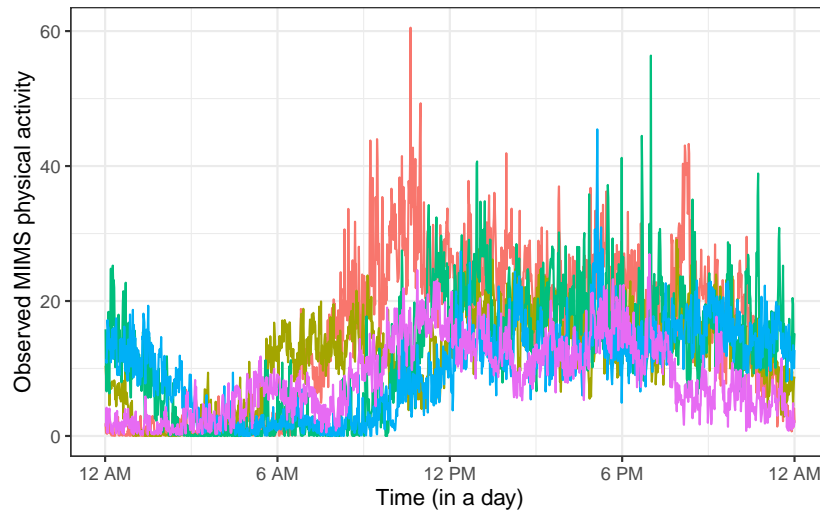


Figure S9: Individual minute-level physical activity counts (MIMS levels) for a few randomly selected participants in the NHANES study conducted by CDC.

To study the impact of age on physical activity, we fit a global Fréchet regression model with estimated force of centrality as functional response and age as predictor. The conditional force of centrality across varying age quantiles is shown in Figure S10. With increasing age, the force of centrality tends to increase steeply to take higher values over a shorter range of minute-level activity counts. Therefore, older participants are less likely to exceed a given MIMS count, which is not surprising.

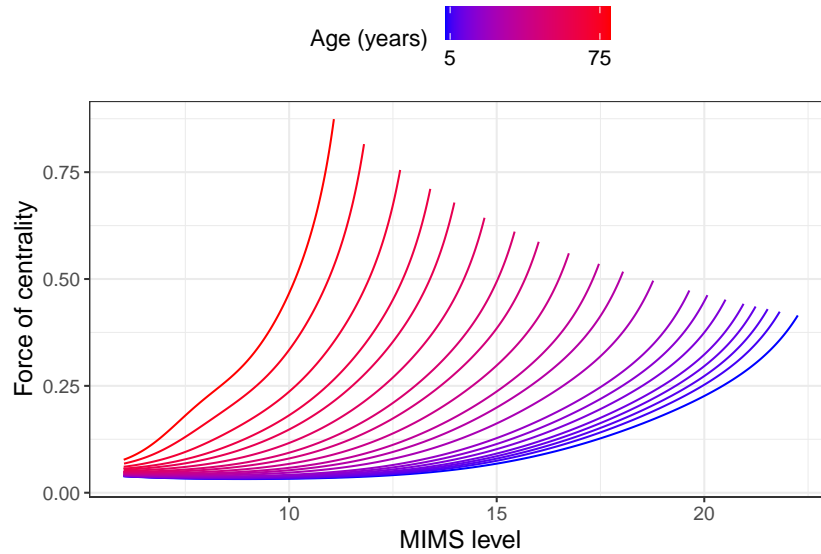


Figure S10: NHANES accelerometer data with minute-level MIMS counts viewed as exceedance levels. Conditional forces of centrality as a function of age, based on fitted global Fréchet regression model.

As further illustrated in Figure S11, for a MIMS count of 11, the threshold exceedance function decreases from 800 minutes at age 5 years to just 200 minutes at age 75 years, demonstrating a sharp decline in physical activity by 75%. These results emphasize the need for age-specific strategies to increase physical activity in older populations (Troiano et al., 2008; Armstrong et al., 2018).

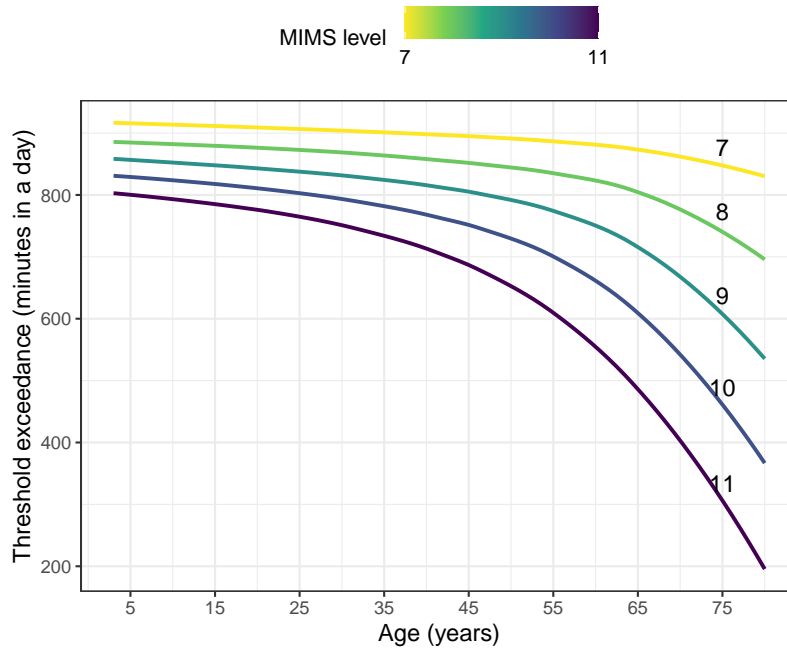


Figure S11: NHANES accelerometer data with minute-level MIMS counts. Conditional threshold exceedance functions at different exceedance levels (minute-level MIMS counts) as a function of age, based on fitted global Fréchet regression model.

Exploring the association between poverty income ratio (continuous predictor) and physical activity using global Fréchet regression, with age group as additional predictor indicates a consistent pattern within each age group: Conditional force of centrality at different PIR quantiles reveals that higher PIR, indicative of wealthier families, are associated with lower MIMS counts, as illustrated in Figure S12. This would reflect that individuals from wealthier backgrounds tend to engage in less physical activity. Furthermore, the effect of PIR is least pronounced in children (age ≤ 12 years) and most prominent in older adults (age > 64 years). This seems to indicate an increasing effect of family socioeconomic status on physical activity levels as individuals age. Moreover, the conditional force of centrality at any given PIR value depicts a trend of higher values over lower MIMS levels when individuals age. This pattern again illustrates the reduced physical activity with increasing age for all socio-economic levels. The threshold exceedance functions depicted in Figure S13 confirm this pattern.

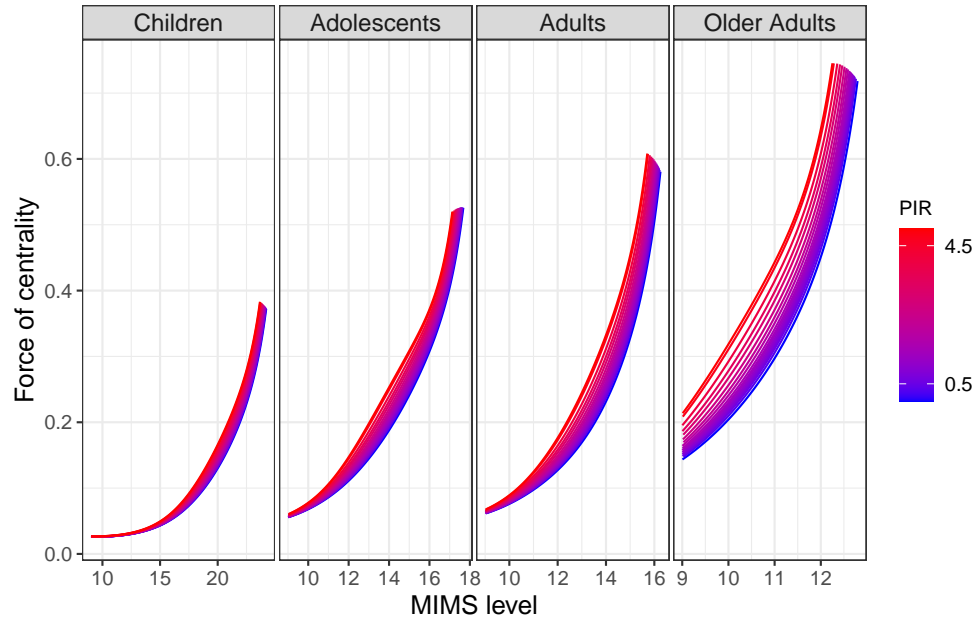


Figure S12: NHANES accelerometer data with minute-level MIMS counts viewed as exceedance levels. Conditional ForCes as a function of poverty income ratio (PIR) for different age groups: children (age ≤ 12 years), adolescents ($12 < \text{age} \leq 19$ years), adults ($19 < \text{age} \leq 64$ years), and older adults (age > 64 years).

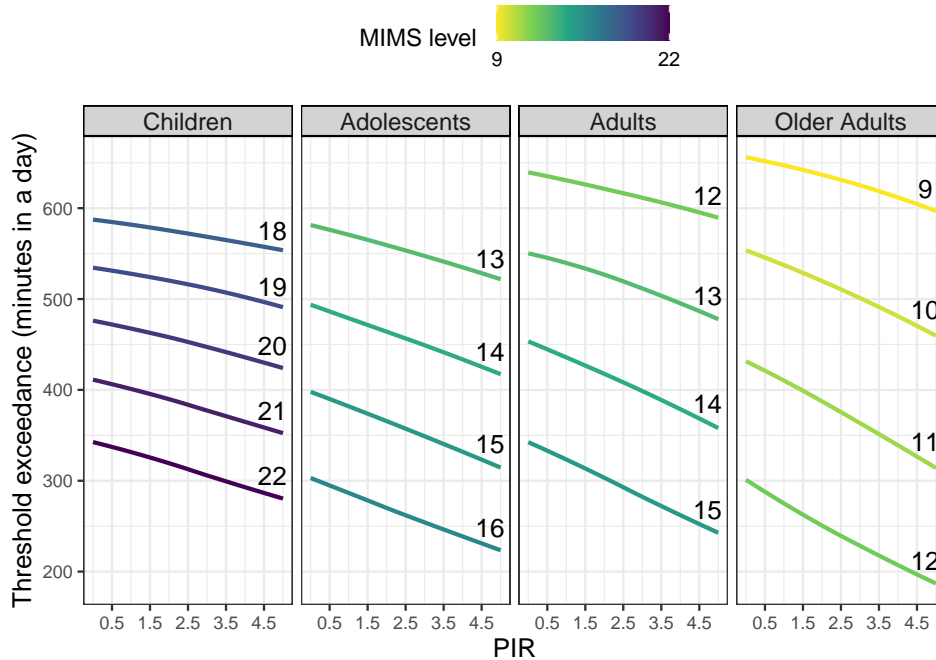


Figure S13: NHANES accelerometer data with minute-level MIMS counts. Conditional threshold exceedance functions at different exceedance levels (minute-level MIMS counts) as a function of poverty income ratio (PIR) for different age groups: children (age ≤ 12 years), adolescents ($12 < \text{age} \leq 19$ years), adults ($19 < \text{age} \leq 64$ years), and older adults (age > 64 years), based on fitted global Fréchet regression model.

To further study the relationship between body weight and physical activity levels (Tudor-Locke et al., 2010), we fit a global Fréchet regression model with BMI as predictor and force of centrality as response. Figure S14 illustrates that participants with higher BMI exhibit steeply increasing force of centrality. This finding aligns with existing literature that associates higher BMI with reduced physical activity.

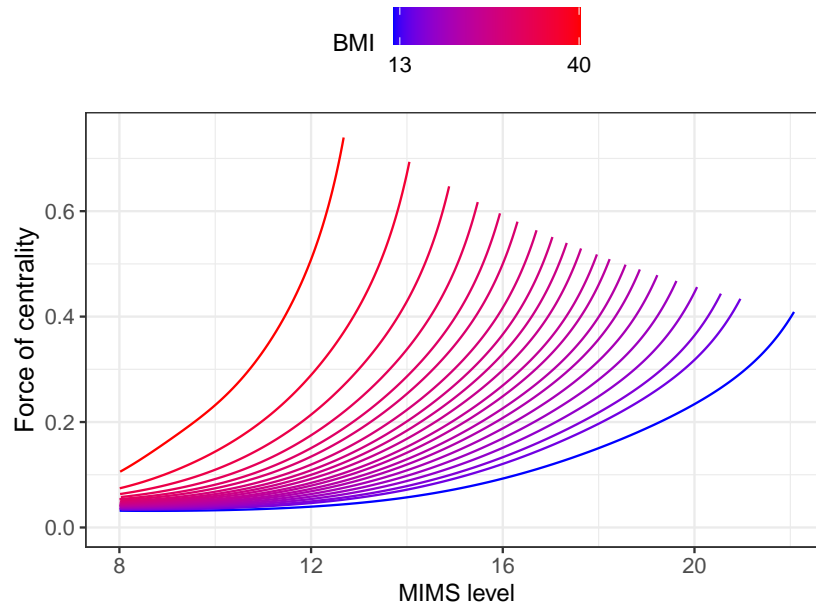


Figure S14: NHANES accelerometer data with minute-level MIMS counts viewed as exceedance levels. Conditional forces of centrality as a function of BMI, based on fitted global Fréchet regression model.

This is also confirmed by the threshold exceedance functions shown in Figure S15. For a MIMS count of 12, the threshold exceedance function decreases from more than 700 minutes at BMI 15 to only 250 minutes at BMI 40.

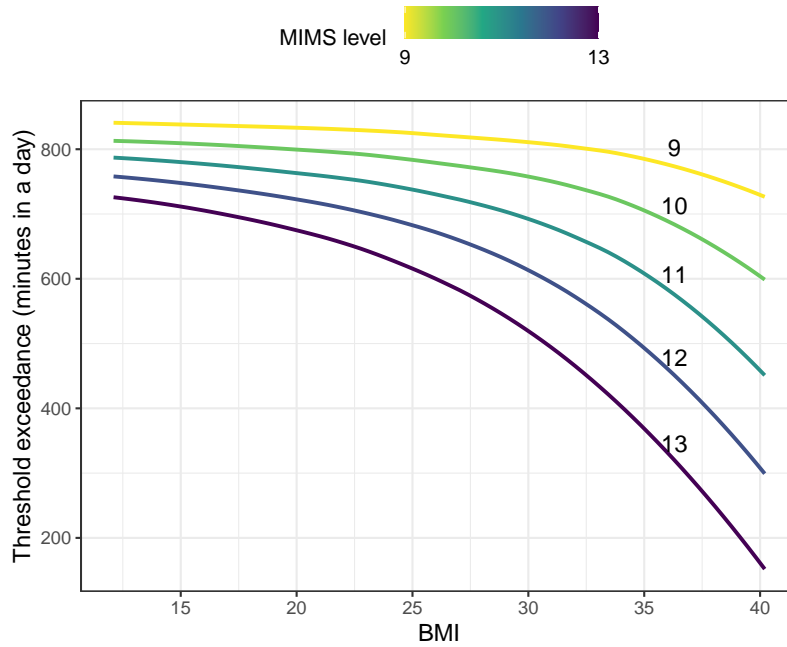


Figure S15: NHANES accelerometer data with minute-level MIMS counts. Conditional threshold exceedance functions at different exceedance levels (minute-level MIMS counts) as a function of BMI, based on fitted global Fréchet regression model.

To identify potential differences in the BMI-activity relationship across different life stages, we incorporate age group as an additional predictor. The results, as illustrated in Figures S16 and S17, reveal a pattern consistent with that in Figure S12.

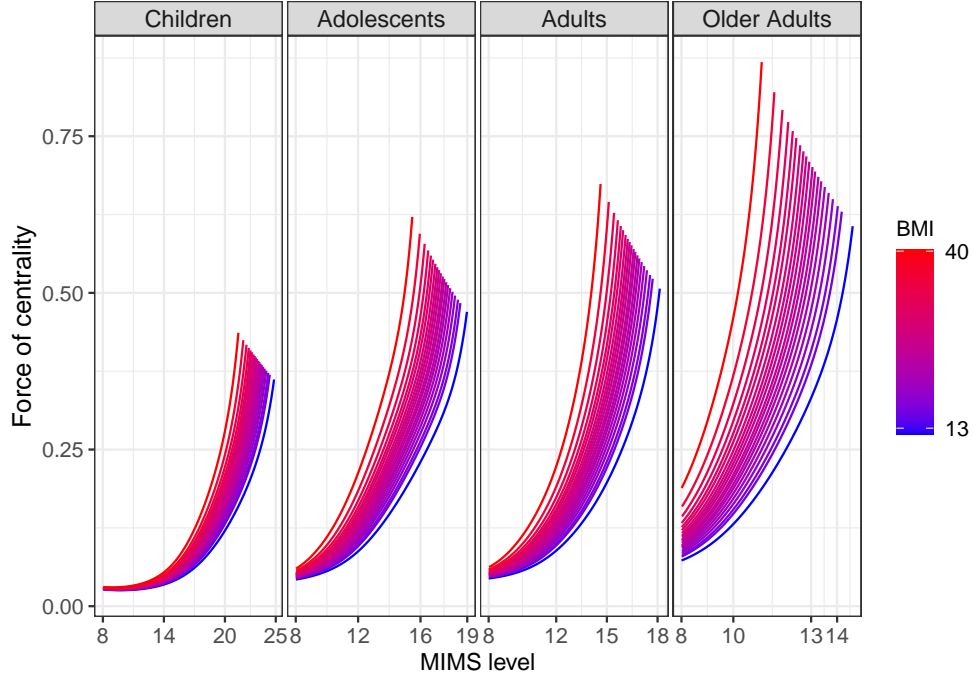


Figure S16: NHANES accelerometer data with minute-level MIMS counts viewed as exceedance levels. Conditional ForCes as a function of BMI for different age groups: children (age ≤ 12 years), adolescents ($12 < \text{age} \leq 19$ years), adults ($19 < \text{age} \leq 64$ years), and older adults (age > 64 years), based on fitted global Fréchet regression model.

S2.2 Additional simulation studies

Table S3: RMSE for conditional threshold exceedance functions based on Fréchet regression models (see Sections 2.2 and 5) for simulation setting I with varying number of subjects n and different number of observations N available per subject, at noise level $\nu_0 = 1$. The reported values (multiplied by 10^3) denote the mean RMSE values averaged over 500 simulation runs, with the corresponding standard errors provided in parentheses.

Model	n	N		
		100	200	500
Global	50	21.032 (5.121)	15.541 (5.082)	14.471 (5.394)
	100	20.626 (4.863)	14.881 (4.835)	13.501 (4.959)
	200	20.400 (4.835)	13.984 (4.684)	13.381 (4.979)
Local	50	12.636 (3.376)	8.461 (3.532)	8.129 (3.272)
	100	11.120 (2.200)	6.326 (2.438)	5.913 (2.226)
	200	10.550 (1.707)	5.094 (1.703)	4.451 (1.527)

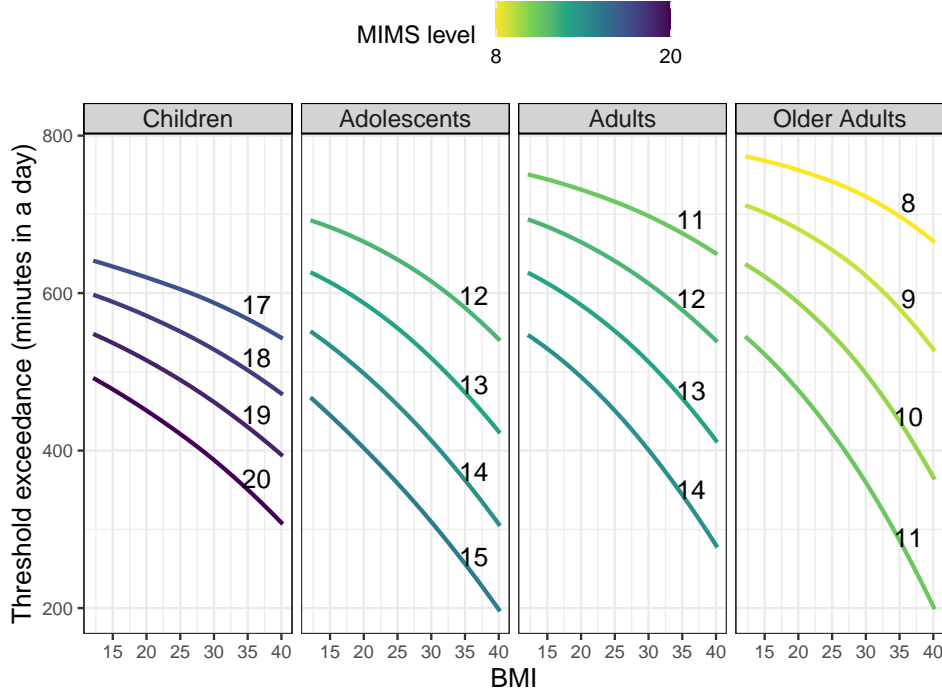


Figure S17: NHANES accelerometer data with minute-level MIMS counts. Conditional threshold exceedance functions at different exceedance levels (minute-level MIMS counts) as a function of BMI for different age groups: children (age ≤ 12 years), adolescents ($12 < \text{age} \leq 19$ years), adults ($19 < \text{age} \leq 64$ years), and older adults (age > 64 years), based on fitted global Fréchet regression model.

To assess the finite-sample performance of global Fréchet regression estimates in Simulation Setting II, we employed a data-generating mechanism analogous to Setting I. With orthonormal basis functions ϕ_k and eigen values λ_k previously used for setting II (see main manuscript), the individual trajectories are constructed via the Karhunen-Loève expansion with white noise $\epsilon_{ij} \stackrel{\text{i.i.d.}}{\sim} \mathcal{N}(0, \nu_0^2)$. Global Fréchet regression is implemented with the parameters $m_0 = 2, a_0 = 1, b_0 = 5, a_1 = 1, b_1 = 5$. For local Fréchet regression, we use $\mu_X = 3, \sigma_X = 0.5, l_X = 1, u_X = 5, m_0 = 2, a_1 = 10, b_1 = 5, c_1 = -3, d_1 = 2$. Figure S22 depicts the results of one simulation run conducted over a dense grid of covariate values with $n = 50, N = 50$, and noise level $\nu_0 = 5$.

References

Armstrong, S., Wong, C. A., Perrin, E., Page, S., Sibley, L., and Skinner, A. (2018). Association of physical activity with income, race/ethnicity, and sex among adolescents and young adults in the

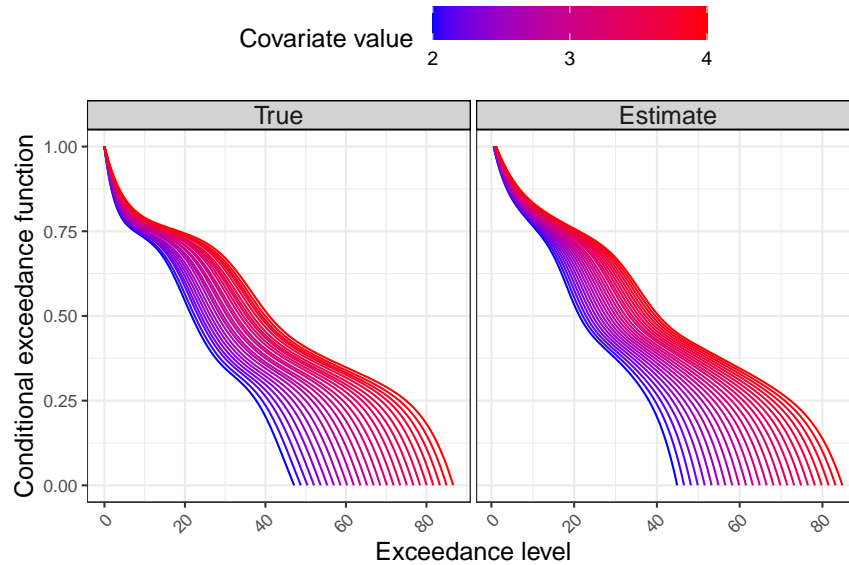


Figure S18: Global Fréchet regression functions (see (19),(20)) for simulation setting I. Conditional exceedance functions (response) for a dense grid of covariate values x , varying from $x = 2$ (blue) to $x = 4$ (red). The left panel displays the “oracle” exceedance functions and the right panel depicts their estimated counterparts.

United States: findings from the National Health and Nutrition Examination Survey, 2007-2016. *Jama Pediatrics*, 172(8):732–740.

Bolstad, B. M., Irizarry, R. A., Åstrand, M., and Speed, T. P. (2003). A comparison of normalization methods for high density oligonucleotide array data based on variance and bias. *Bioinformatics*, 19(2):185–193.

Burke, M., Hsiang, S. M., and Miguel, E. (2015). Global non-linear effect of temperature on economic production. *Nature*, 527(7577):235–239.

Cai, T. T. and Hall, P. (2006). Prediction in functional linear regression. *The Annals of Statistics*, 34(5):2159–2179.

Cai, T. T. and Yuan, M. (2011). Optimal estimation of the mean function based on discretely sampled functional data: Phase transition. *The Annals of Statistics*, 39(5):2330–2355.

Chang, H.-W. and McKeague, I. W. (2022). Empirical likelihood-based inference for functional means with application to wearable device data. *Journal of the Royal Statistical Society Series B: Statistical Methodology*, 84(5):1947–1968.

Chen, H., Müller, H.-G., Rodovitis, V. G., Papadopoulos, N. T., and Carey, J. R. (2024). Daily activity profiles over the lifespan of female medflies as biomarkers of aging and longevity. *Aging Cell*, page e14080.

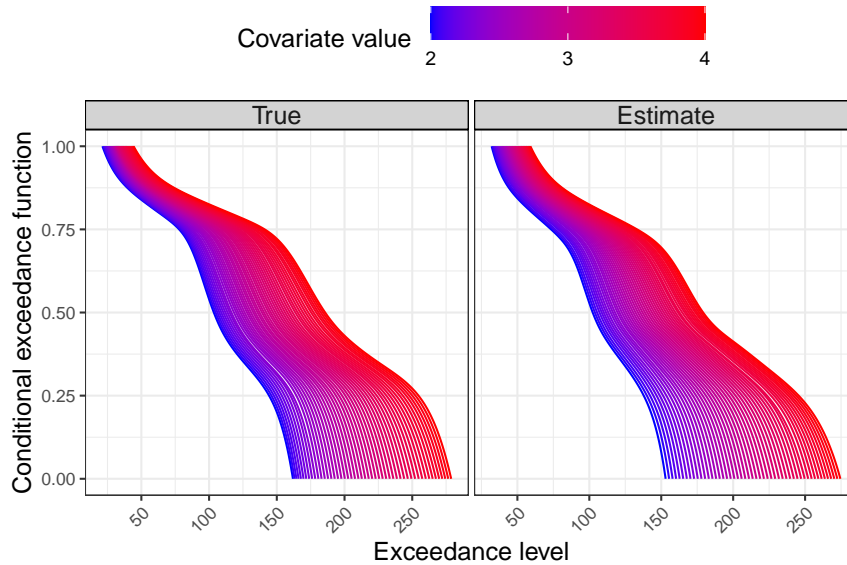


Figure S19: Local Fréchet regression functions (see (17), (18)) for simulation setting I. Conditional exceedance functions (response) for a dense grid of covariate values x , varying from $x = 2$ (blue) to $x = 4$ (red). The left panel displays the “oracle” exceedance functions and the right panel depicts their estimated counterparts.

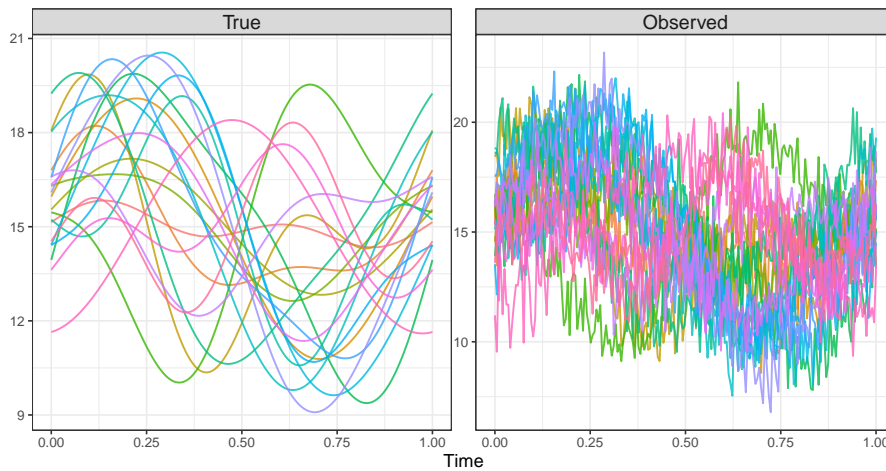


Figure S20: Simulation setting II. True underlying trajectories (left) and observed data (right) for 20 randomly selected subjects and noise variance 1.

Chen, Y. and Müller, H.-G. (2022). Uniform convergence of local Fréchet regression with applications to locating extrema and time warping for metric space valued trajectories. *The Annals of Statistics*, 50(3):1573–1592.

Crainiceanu, C. M., Goldsmith, J., Leroux, A., and Cui, E. (2024). *Functional data analysis with R*. CRC Press.

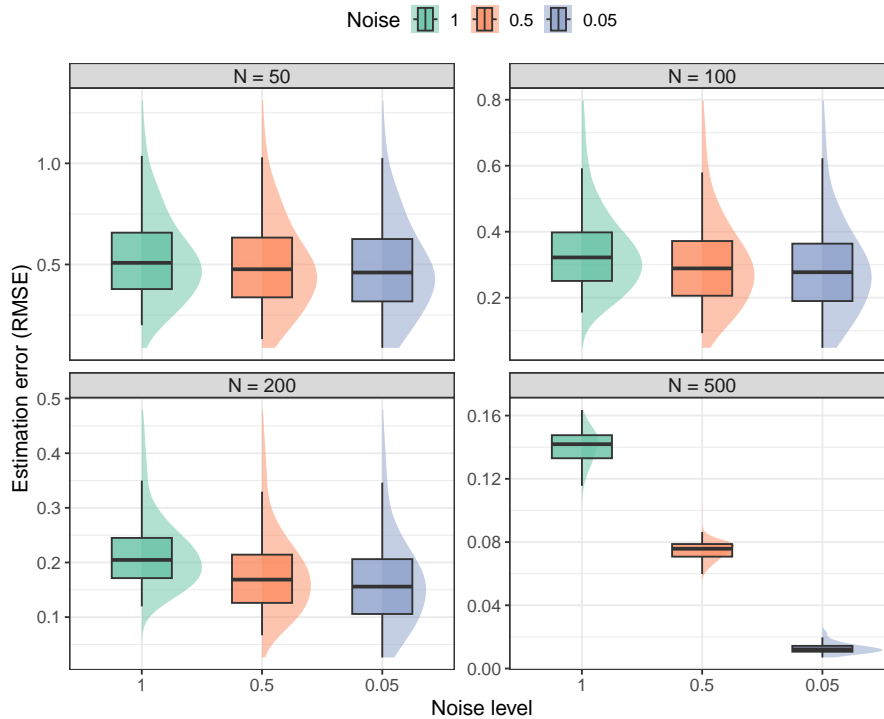


Figure S21: Individual-level RMSE for each of the $n = 200$ subjects averaged over 1000 simulation runs for the estimation of exceedance functions (defined in Section 4) in simulation setting II with varying number of observations N available per subject and varying noise level ν_0 .

Davariashtiyani, A., Taherkhani, M., Fattahpour, S., and Vitousek, S. (2023). Exponential increases in high-temperature extremes in North America. *Scientific Reports*, 13(1):19177.

Drufuca, G. and Giugliano, M. (1977). The duration of high SO_2 concentrations in an urban atmosphere. *Atmospheric Environment (1967)*, 11(8):729–735.

Ebi, K. L., Capon, A., Berry, P., Broderick, C., de Dear, R., Havenith, G., Honda, Y., Kovats, R. S., Ma, W., Malik, A., et al. (2021). Hot weather and heat extremes: health risks. *The lancet*, 398(10301):698–708.

Fan, J. and Gijbels, I. (1996). *Local Polynomial Modelling and Its Applications: Monographs on Statistics and Applied Probability 66*, volume 66. CRC Press.

Ferraty, F. and Vieu, P. (2006). *Nonparametric Functional Data Analysis: Theory and Practice*. Springer Science & Business Media.

Gilleland, E. and Katz, R. W. (2016). *extRemes 2.0: An Extreme Value Analysis Package in R*.

Graham, C. (1982). The parameterisation and prediction of wave height and wind speed persistence statistics for oil industry operational planning purposes. *Coastal Engineering*, 6(4):303–329.

Hall, P. and Horowitz, J. L. (2007). Methodology and convergence rates for functional linear regression. *The Annals of Statistics*, 35(1):70–91.

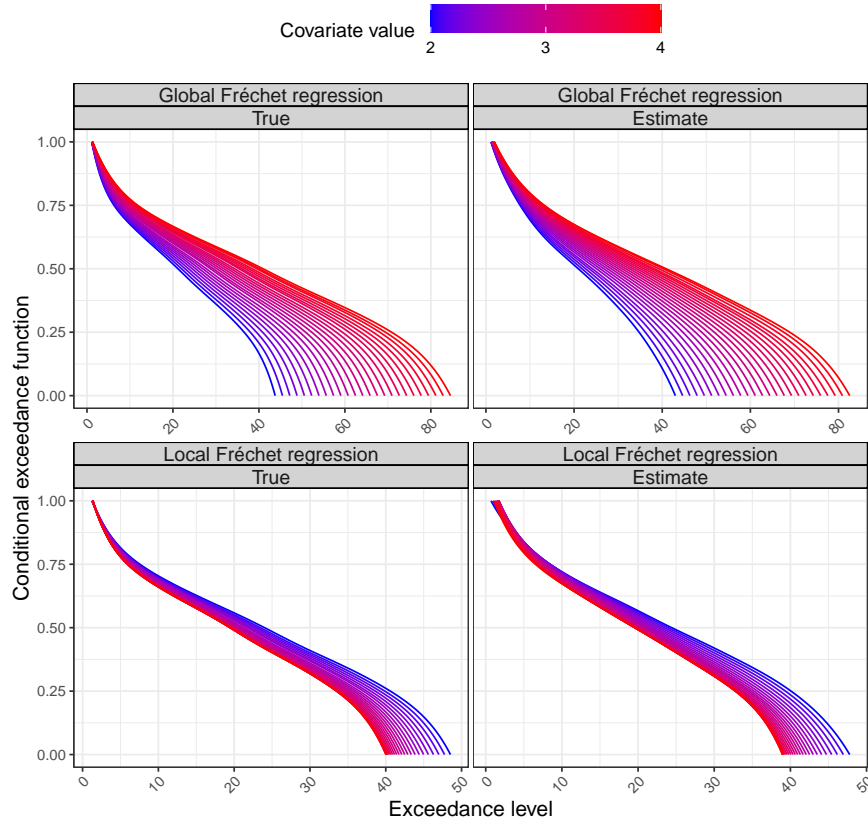


Figure S22: Global (top panel) and local (bottom panel) Fréchet regression functions for simulation setting II. Conditional exceedance functions (response) for a dense grid of covariate values x , varying from $x = 2$ (blue) to $x = 4$ (red). The left panel displays the “oracle” exceedance functions and the right panel depicts their estimated counterparts.

Hall, P., Müller, H.-G., and Wang, J.-L. (2006). Properties of principal component methods for functional and longitudinal data analysis. *The Annals of Statistics*, 34(3):1493–1517.

Horváth, L. and Kokoszka, P. (2012). *Inference for Functional Data with Applications*, volume 200. Springer Science & Business Media.

Hsing, T. and Eubank, R. (2015). *Theoretical Foundations of Functional Data Analysis, with an Introduction to Linear Operators*. John Wiley & Sons.

Iao, S. I., Kundu, P., Chen, H., Carey, J. R., and Müller, H.-G. (2024). Longitudinal activity monitoring and lifespan: quantifying the interface. *Aging*, 16:12108–12122.

Müller, H.-G. (1987). Weighted local regression and kernel methods for nonparametric curve fitting. *Journal of the American Association*, 82(397):231–238.

Petersen, A. and Müller, H.-G. (2019). Fréchet regression for random objects with Euclidean predictors. *The Annals of Statistics*, 47(2):691–719.

Ramsay, J. and Silverman, B. (2006). *Functional Data Analysis*. Springer Science & Business Media.

- Rice, J. A. and Wu, C. O. (2001). Nonparametric mixed effects models for unequally sampled noisy curves. *Biometrics*, 57(1):253–259.
- Schrack, J., Zhang, T., Wanigatunga, A., Zipunnikov, V., and Freedman, V. (2023). Accelerometer-derived physical activity in the national health and aging trends study. *Innovation in Aging*, 7:165–166.
- Shao, L., Lin, Z., and Yao, F. (2022). Intrinsic riemannian functional data analysis for sparse longitudinal observations. *The Annals of Statistics*, 50(3):1696–1721.
- Tabacu, L., Ledbetter, M., Leroux, A., Crainiceanu, C., and Smirnova, E. (2020). Quantifying the varying predictive value of physical activity measures obtained from wearable accelerometers on all-cause mortality over short to medium time horizons in NHANES 2003–2006. *Sensors*, 21(1):4.
- Troiano, R. P., Berrigan, D., Dodd, K. W., Masse, L. C., Tilert, T., McDowell, M., et al. (2008). Physical activity in the United States measured by accelerometer. *Medicine and science in sports and exercise*, 40(1):181.
- Tudor-Locke, C., Brashear, M. M., Johnson, W. D., and Katzmarzyk, P. T. (2010). Accelerometer profiles of physical activity and inactivity in normal weight, overweight, and obese US men and women. *International Journal of Behavioral Nutrition and Physical Activity*, 7:1–11.
- Wang, J.-L., Chiou, J.-M., and Müller, H.-G. (2016). Functional data analysis. *Annual Review of Statistics and Its Application*, 3:257–295.
- Yao, F. and Lee, T. C. (2006). Penalized spline models for functional principal component analysis. *Journal of the Royal Statistical Society Series B: Statistical Methodology*, 68(1):3–25.
- Yao, F., Müller, H.-G., and Wang, J.-L. (2005a). Functional data analysis for sparse longitudinal data. *Journal of the American Statistical Association*, 100(470):577–590.
- Yao, F., Müller, H.-G., and Wang, J.-L. (2005b). Functional linear regression analysis for longitudinal data. *The Annals of Statistics*, 33(6):2873–2903.
- Yuan, M. and Cai, T. T. (2010). A reproducing kernel hilbert space approach to functional linear regression. *The Annals of Statistics*, 38(6):3412–3444.
- Zhang, X. and Wang, J.-L. (2016). From sparse to dense functional data and beyond. *The Annals of Statistics*, 44(5):2281–2321.
- Zhang, Z. and Müller, H.-G. (2011). Functional density synchronization. *Computational Statistics & Data Analysis*, 55(7):2234–2249.